INVESTIGATION OF THE EFFECT OF DESIGN PARAMETERS ON VAPOR CHAMBER HEAT TRANSFER CHARACTERISTIC

A THESIS SUBMITTED TO
THE GRADUATE SCHOOL OF NATURAL AND APPLIED SCIENCES
OF
MIDDLE EAST TECHNICAL UNIVERSITY

BY

İREM KARAKAYA

IN PARTIAL FULFILLMENT OF THE REQUIREMENTS
FOR
THE DEGREE OF MASTER OF SCIENCE
IN
MECHANICAL ENGINEERING

NOVEMBER 2022

Approval of the thesis:

INVESTIGATION OF THE EFFECT OF DESIGN PARAMETERS ON VAPOR CHAMBER HEAT TRANSFER CHARACTERISTIC

submitted by **İREM KARAKAYA** in partial fulfillment of the requirements for the degree of **Master of Science in Mechanical Engineering Department, Middle East Technical University** by,

Prof. Dr. Halil Kalıpçılar
Dean, Graduate School of **Natural and Applied Sciences** _____

Prof. Dr. Mehmet Ali Sahir Arıkan
Head of Department, **Mechanical Engineering** _____

Assoc. Prof. Dr. Özgür Bayer
Supervisor, **Mechanical Engineering, METU** _____

Prof. Dr. Zafer Dursunkaya
Co-supervisor, **Mechanical Engineering, METU** _____

Examining Committee Members:

Prof. Dr. Almıla Güvenç Yazıcıoğlu
Mechanical Engineering, METU _____

Assoc. Prof. Dr. Özgür Bayer
Mechanical Engineering, METU _____

Prof. Dr. Zafer Dursunkaya
Mechanical Engineering, METU _____

Prof. Dr. Murat Köksal
Mechanical Engineering, Hacettepe University _____

Assist. Prof. Dr. Altuğ Özçelikkale
Mechanical Engineering, METU _____

Date: 25.11.2022

I hereby declare that all information in this document has been obtained and presented in accordance with academic rules and ethical conduct. I also declare that, as required by these rules and conduct, I have fully cited and referenced all material and results that are not original to this work.

Name, Surname: İrem Karakaya

Signature :

ABSTRACT

INVESTIGATION OF THE EFFECT OF DESIGN PARAMETERS ON VAPOR CHAMBER HEAT TRANSFER CHARACTERISTIC

Karakaya, İrem
M.S., Department of Mechanical Engineering
Supervisor: Assoc. Prof. Dr. Özgür Bayer
Co-Supervisor: Prof. Dr. Zafer Dursunkaya

November 2022, 63 pages

In this study, a detailed two-phase computational modeling of a vapor chamber is performed. A code written in MATLAB is used to accurately simulate the phase-change process within the wick structure. Conservation of mass is satisfied by matching the evaporated and condensed fluid mass flow rates. Secant Method is used to find vapor temperature. The current model is validated and then, wall temperature, pressure, and mass flow rate distributions of the working fluid are calculated and plotted. Parametric study is performed to see the effects of operating and design parameters on the vapor chamber heat transfer and fluid flow characteristics. In this parametric study, porosity, wick and wall thicknesses, wall material, different working fluid, and material types are investigated. According to the specifications of the design, the dry-out condition is evaluated through a comparison of the liquid pressure drop and the capillary pressure head. It is examined if the maximum system temperature exceeds the maximum allowable temperature. Parametric results show that in order to achieve the desired conditions of a lower temperature drop in the system and a higher dry-out heat flux condition, the best vapor chamber design parameter set for given design

conditions in the current study, consists of copper-water as a working fluid and material couple, smaller porosity (0.45), smaller wick thickness (0.12 mm), and larger wall thickness (0.25 mm). The current vapor chamber model enables to specify the parameters to design a vapor chamber.

Keywords: Vapor chamber, wick, two-phase cooling, electronics cooling, phase-change modeling

ÖZ

TASARIM PARAMETRELERİNİN BUHAR ODASININ ISI AKTARIM ÖZELLİKLERİ ÜZERİNE ETKİSİNİN İNCELENMESİ

Karakaya, İrem
Yüksek Lisans, Makina Mühendisliği Bölümü
Tez Yöneticisi: Doç. Dr. Özgür Bayer
Ortak Tez Yöneticisi: Prof. Dr. Zafer Dursunkaya

Kasım 2022 , 63 sayfa

Bu çalışmada, bir buhar odasının ayrıntılı ve yeni iki fazlı hesaplama modellemesi gerçekleştirilmiştir. MATLAB ortamında fitil yapısındaki faz değiştirme sürecini simüle etmek bir kod geliştirilmiştir. Kütlenin korunması, buharlaşan ve yoğunlaşan sıvı kütle akış hızlarının eşleşmesiyle sağlanır. Sekant metodu buhar sıcaklığını bulmak için kullanılmıştır. Mevcut model doğrulanıp ve ardından çalışma sıvısının duvar sıcaklığı, basıncı ve kütle akış hızı dağılımları hesaplanmış ve çizilmiştir. Ayrıca, çalışma ve tasarım parametrelerinin buhar odası ısı aktarımı ve sıvı akış özellikleri üzerindeki etkilerini görmek için parametrik bir çalışma gerçekleştirilmiştir. Bu parametrik çalışmada gözeneklilik, fitil ve duvar kalınlıkları, duvar malzemesi, farklı çalışma sıvısı ve malzeme türleri incelenmiştir. Tasarımın özelliklerine uygun olarak kuruma durumu, sıvı basınç düşüşü ve kılcal basınç yüksekliğinin karşılaştırılmasıyla değerlendirilmiştir. Maksimum sistem sıcaklığının, sistemin izin verilen maksimum sıcaklığını aşıp aşmadığı incelenmiştir. Parametrik sonuçlara göre, sistemde daha düşük sıcaklık düşüşü ve daha yüksek kuruma ısı akısı koşulunun istenen koşullarını

elde etmek için mevcut çalışmada verilen tasarım koşullarına göre en iyi buhar odası tasarımı parametre seti, çalışma sıvısı ve malzeme çifti olarak bakır-su, daha küçük gözeneklilik (0.45), daha küçük fitil kalınlığı (0.12 mm) ve daha büyük duvar kalınlığı (0.25 mm) olarak belirlenebilir. Mevcut buhar odası modeli bir buhar odası tasarlamak için parametrelerin belirlenmesini sağlar.

Anahtar Kelimeler: Buhar odası fitil, iki fazlı soğutma, elektronik soğutma, faz değişimi modellenmesi

To my family

ACKNOWLEDGMENTS

First and foremost I would like to be extremely grateful to my supervisors Prof. Dr. Zafer Dursunkaya and Assoc. Prof. Dr. Özgür Bayer for their invaluable advice and criticism, encouragements, continuous support, and patience during this thesis.

I would like to express my deepest gratitude to all members of Dr. Bayer's Research Group.

Special thanks goes to Ayse Uğur, for her help, late-night feedback and moral support.

Finally, I am extremely grateful to my parents and my brother, I could not have undertaken this journey without their support.

TABLE OF CONTENTS

LIST OF TABLES

TABLES

LIST OF FIGURES

FIGURES

LIST OF ABBREVIATIONS

2D	2 Dimensional
3D	3 Dimensional
CFD	Computational Fluid Dynamics
DOE	Design of Experiments
HTC	Heat Transfer Coefficient
TC	Thermal Conductivity
VC	Vapor Chamber
VCHS	Vapor Chamber Heat Spreaders

LIST OF SYMBOLS

A	Area, m^2
c_p	Specific heat capacity, kJ/(kg·K)
C	Coefficient, -
d	Diameter, mm
f	Friction factor, -
H	Height, mm
h	Heat transfer coefficient, W/(m^2·K)
h_{fg}	Latent heat of evaporation, J/kg
k	Thermal conductivity, W/(m·K)
K	Permeability, m^2
L	Length, mm
$\dot{m}$	Mass flow rate, kg/s
$\dot{m}''$	Mass flux, kg/(m^2·s)
M	Molecular weight, kg/mol
P	Pressure, Pa
q	Heat flow rate, W
$\dot{q}$	Heat generation rate, W/m^3
r	Radius, mm
R_u	Universal gas constant, J/(mol·K)
R	Thermal resistance, K/W
T	Temperature, K
u	Velocity in x-direction, m/s
v	Velocity in y-direction, m/s

y	Thickness, mm

Greek Symbols

Δ	Finite difference
ε	Porosity, -
ϵ	Accuracy, -
τ	Shear stress, Pa
$\hat{\sigma}$	Accommodation coefficient, -
σ	Surface tension, N/m
ρ	Density, kg/m^3
ν	Specific volume, m^3/kg
μ	Dynamic viscosity, (N·s)/m^2

LIST OF SUBSCRIPTS

$adia$	Adiabatic
amb	Ambient
ax	Axial
b	Wall
c	Capillary
$cond$	Condenser
eff	Effective
$evap$	Evaporator
gr	Gravity
hsi	Heat sink
hs	Heat source
int	Interface
i	i^{th} control volume
lat	Lateral
l	Liquid
lv	Liquid-vapor
p	Pore
s	Solid
v	Vapour
w	Wick

CHAPTER 1

INTRODUCTION

1.1 Research Overview

In the past, the thermal management of electrical and mechanical systems has presented challenges to thermal designers. Heat is an unavoidable aspect of any electronic system, and high operating temperatures are detrimental to performance and result in mechanical failures due to thermal expansion problems [1, 2]. Therefore, effective cooling requirements and thermal management of the electronic devices, components, and packages are essential concerns for the continued safe and efficient operation of the systems. In the first studies on the thermal management of electronic equipment, natural or forced convection was used by utilizing an external heat sink on the equipment to create more surface area to release heat [3]. Heat conducts through these heat sinks, which are made from common materials such as copper and aluminum, and heat is released through natural or forced convection.

According to the applications, the types of fins and heat sinks, as well as their dimensions can vary. However, increasing the size and weight of heat sinks is not an option for most applications. The size and type of fans that can be used on a heat sink are often constrained by factors like board space, weight, and manufacturing costs. In real-world applications, simply increasing the size of the heat sink and the airflow is not always a viable solution, even if the design requirements permit it. A heat sink that is too large or an airflow that is too high will limit the possible improvements that could be applied to thermal performance. At some point existing equipment will not satisfy the thermal requirements of the new generation electrical and mechanical devices. The heat sink size, airflow, or other traditional cooling methods will reach

their limits at that point. On the other hand, this is not sufficient to cool electronic components because the heat dissipation capacity is insufficient in this kind of heat conduction technique. In addition to that, most of these techniques utilize active cooling, which needs power to perform its duty. The more heat is generated, the more cooling is needed. With advances in the electronics technology, the dissipated heat in electronic devices has become so large that the traditional techniques cannot keep up with it. Therefore, new alternative methods and techniques have emerged in the area of effective cooling.

Nowadays, most electronic devices are based on chipsets. This technology significantly increases the frequency and power of electronic components. This means that the larger power density of these devices causes higher temperatures, thermal expansion and thermal fracture [4]. While the size of electronic devices is getting smaller, heat release has accumulated at a single location. These locations can cause thermal failure of components, so they must be avoided by employing appropriate cooling strategies. While traditional cooling techniques have been used successfully until now, other cooling solutions are needed to meet the challenges of higher heat fluxes. To overcome the requirements for more cooling power, two-phase cooling heat transport systems have been used over the decades [5]. Since the year 1963, when the first heat pipe was created, sufficient thermal capabilities of heat pipes have been revealed as a result of experimental studies [6]. Heat pipes have been used for a long time in desktop computers, laptops, and mobile devices for removal of heat.

A heat pipe is a closed container. The basic principle of the heat pipe is the circulation of the fluid between the heat source and heat sink regions, as well as the adiabatic region between these parts. Fluid flow cycles between these sides through the porous material which is called a wick. A heat source generates heat and the working fluid evaporates throughout this region. Vapor flows go to the heat sink region due to the generated pressure and temperature difference. Then the condensed fluid returns passively to the heat source region under vacuum by ejecting its latent heat to the heat sink or any other external device. The wick structure inside the heat pipe enables fluid to circulate inside the heat pipe by using capillary action. Figure 1.1 presents the heat pipe design and working cycle. The transition mechanism between liquid and vapor phases is very effective and continues fluently unless the design limitations, which

are associated with the working fluid and wick type parameters, have been exceeded.

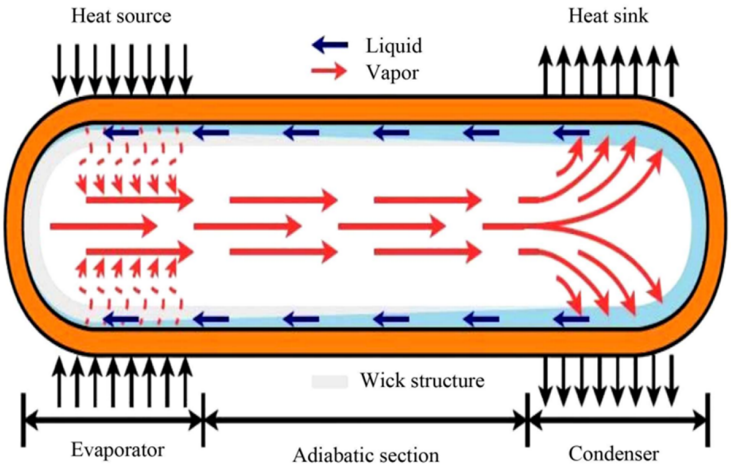

Figure 1.1: Heat pipe design and working cycle [7]

Another type of two-phase cooling device is the vapor chamber (VC). Heat pipes have been used for a long time to help with heat management, but VCs haven't been common until recently. The VC is a new type of two-phase heat transfer device that often resembles a thin piece of metal. There has been significant progress in the study of VCs. VCs are now thinner and more lightweight compared to past years, and engineers are discovering numerous new ways to incorporate them into cooling systems.

The working principle of the vapor chamber is similar to that of the heat pipe. As observed in heat pipes, there are the same sections in the vapor chamber such as the heat source and the heat sink, as well as the same dynamic systems for fluid circulation in terms of evaporation and condensation as observed in heat pipes. As shown in Figure 1.2, at the bottom section of the vapor chamber, heat comes from a heat source, which causes the working fluid to evaporate. Evaporated working fluid goes to the heat sink region, where it releases heat, and the condensed liquid turns back to the heat source region because of capillary effect through the wick on the sides or turns back as droplets via gravity. On the other hand, the vapor chamber separates from the heat pipe in terms of heat spreading direction. A heat pipe spreads the heat along the axis and works better at cooling discrete heat sources. A vapor chamber has

two-dimensional heat spreading capability, and they are mostly used for high power applications and heat fluxes from a small evaporator field to a larger heat sink. Also, the vapor chamber prevents hot spots by spreading heat in two dimensions to a heat sink, which has a larger area. There are many factors that make them particularly an excellent choice for the cooling of electronics, such as being lightweight, withstanding the high heat flux of the devices, good and reliable performance, etc.

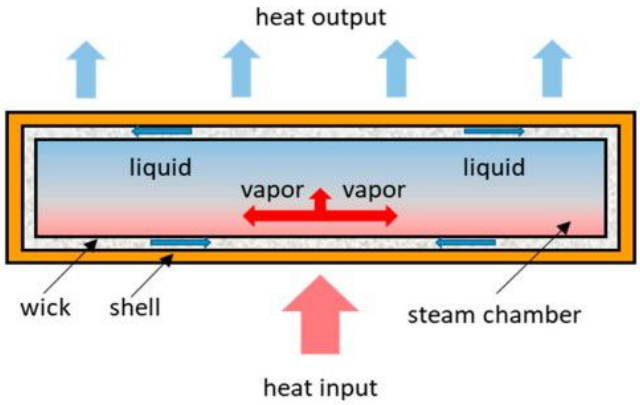

Figure 1.2: Vapor chamber scheme and working cycle [8]

When integrated into heat sinks, vapor chambers can transfer heat in all directions, reducing spreading resistance and allowing for more efficient heat transfer. By exploiting these features of vapor chambers the performance can be improved by lowering the total thermal resistance of a heat management solution. To prove this, Nguyen compared the thermal resistances of the vapor chamber and the copper system and he discovered that while the total thermal resistance was 0.25 K/W for the vapor chamber, the thermal resistance of the copper base system was 0.31 K/W [9].

The statements above point out that the phase change mechanism between liquid and vapor and the flow through the porous medium have significantly more impact on the heat transfer process than traditional cooling techniques, which rely on simple heat conduction between solid components. Therefore, there are many fluid flow and heat transfer mechanisms involved in operation of the two-phase devices. This leads to a complex problem of coupled fluid flow and heat transfer. In addition to that, many parameters influence the performance such as working fluid type, wick material, charge ratio, etc. This also means that investigation of these parameters is critical

to designing and analyzing for thermal management performance. It is difficult to figure out how to control the temperature and to decide how each parameter affects the overall performance. This is true both for solving the problems analytically and numerically. Due to its heat spreading capability and and its practical applications for electronic-based technologies, the vapor chamber has been selected for this study and will be explored in detail to inspect design and fluid parameters. This work focuses on vapor chamber modeling in order to investigate the influence of these parameters on the thermal and flow characteristics of the vapor chambers.

1.2 Literature Review on Vapor Chambers

In recent years, there have been many studies on vapor chambers due to the popularity of thermal management concerns in electronic devices, since keeping these systems safe and efficient. As a traditional method, the external heat sink is used for thermal management. It enables to reduce the thermal resistance while dissipating the heat. As a result, higher heat loads can be transferred while still maintaining safe operating temperatures. Generally, these kinds of structures are constructed of copper or aluminum materials. Heat comes to the heat sink through conduction, and then heat is removed by natural or forced convection [10]. Fans are generally used for the purpose of forced convection. Besides the traditional methods, phase change heat transfer devices, such as heat pipes and vapour chambers are commonly employed to increase the efficiency of thermal performance.

To investigate the thermal-flow behavior of the vapor chambers, besides experimental methods, modeling approaches are needed because experiments can take a long time to design, manufacture, and collect the data. On the other hand, modeling via analytical or numerical methods is beneficial for determining the design parameters as well as optimizing these parameters according to the purpose of their use.

In the literature, some modeling approaches have been performed for the working principle of the vapor chamber. Although modeling a vapor chamber is complicated by the device's coupled heat, mass, and momentum transport mechanisms, such as evaporation and condensation at the liquid vapor interfaces, a variety of modeling

approaches, such as analytical and numerical, have been developed. Prasher et al. demonstrated that the conduction-based model was developed on the basis of some simplifying assumptions with temperature reductions owing to the wick and vapour region [11]. In this work, a remote cooling mode where the heat sink was located at the farthest point of the vapor chamber, such as at the end of the top wall of the vapor chamber, was used in the experimental setup. It was found the heat transport capacity and thermal resistance were based on a conduction model. This work was validated by experiments and showed good agreement, so this work was very beneficial for people who design and optimize heat pipe and vapor chamber products. Vadakkan et al. developed a steady-state and transient CFD model by taking-into consideration wick-vapor interface phase change phenomena according to kinetic energy theory [12]. To calculate the pressure drop of the fluid flow inside the wick, the Brinkman-Forchheimer extended Darcy model was used. In this model, single and multiple heat sources were used. This model was beneficial in finding the value of heat flux that caused the dry-out as well as the location where the dry-out occurred. To avoid dry out conditions, the optimum wick structure was studied to enable the vapor chamber to have an optimum pressure drop. Besides the dry-out condition, capillary requirements were investigated. Wei et al., studied a multiblock approach for modeling the vapor chamber to observe the thermal management effectiveness and sensitivity of the vapor chamber [13]. The multiblock consisted of wick, vapor, thermal interface material, heat source, and heat sink. It was demonstrated that the model was capable of accurately predicting the temperature profile when compared to the findings of a thorough numerical model. According to the results, thermal performance was affected by the wick thermal conductivity. Wang and Vafai modeled the vapor chamber under transient conditions for startup and shutdown conditions by using an analytical method [14]. The results of both experiments and the validated model showed that the total thermal resistance of the vapor chamber was mainly affected by wick parameters. The heat transfer coefficient had the most influence on reaching a steady state condition of the system. Hsieh et al. developed a three-dimensional analytical model [15]. This model was solved using the method of separation of variables. A parametric study was performed, and it showed how the design parameters such as thickness and height with pillar and without pillar have effects on the thermal performance of the vapor chamber. Koito et al. developed

a mathematical model of a disk-shaped vapor chamber in this paper with the finite volume method [16]. The numerical results were validated with experimental results. Continuity, momentum, and energy equations were solved by using the SIMPLE algorithm. According to the results, temperature uniformity was observed at the top of the vapor chamber. Ming et al. designed a vapor chamber that has a grooved type of wick structure [17]. Numerical and experimental studies were performed, and the results showed that this type of wick structure provided uniform heat transfer in both axial and radial directions. Additionally, the two-dimensional numerical model provided an investigation of the liquid distribution inside the wick's grooved channel. Experimental results showed that dry-out condition and poor thermal performance were observed when the heat flux became larger. The magnitudes of liquid and vapor velocities depended on the heat flux value. Due to the higher velocity of vapor, higher pressure drops were observed compared to liquid pressure drop. Zhu and Vafai performed studies on an asymmetrical flat plate heat pipe [18]. They developed both three-dimensional analytic and numerical models. Non-Darcian effects on pressure drop inside the wick structure and gravitational effects were taken into consideration. The numerical model was carried out by using the finite element method with the Galerkin method. It is worth noting that there was very strong agreement between the analytical and numerical results in terms of qualitative and quantitative parameters. Patankar et al. carried out a study that was about the transient characteristics of the vapor chamber [19]. A model that included the time dependent heat flux was developed because understanding the thermal behavior of a vapor chamber is crucial. Additionally, a parametric study according to the thickness of the wall, wick, and vapor regions was performed, and the effect of the working fluid was investigated. The study showed that the optimization approach for the thickness of the wall, wick, and vapor sides under steady state conditions was different than the transient conditions due to a number of governing mechanisms. Peterson et al. developed a numerical model of a novel sandwich panel heat pipe with a non-uniform heat flux by using the finite volume method for the wall, wick, and vapor regions [20]. On the heat sink side, natural convection with a constant heat transfer coefficient and radiative heat transfers were taken into consideration. The thermal characteristics of the model were investigated. Experimental results were in good agreement with numerical results. Results showed that the heat sink side of the model had good temperature uniformity. Rice

and Faghri developed a numerical model of a heat pipe with single and multiple heat sources for both flat-plate and cylindrical geometries [21]. Radiative and convective boundary conditions were considered on the heat sink side. On the other hand, a maximum capillary pressure study was performed to investigate whether dry-out occurs or not for a given heating load. A number of heating settings and power levels were used to determine the capillary pressure required in the wick to push the flow of fluid inside the wick structure. Also, the model presented mass flux variation at the liquid-vapor interface by using single-pore analysis without any empirical methods. Naphon et al. performed both experimental and numerical studies to investigate the effect of the micro-channel on the vapor chamber [22]. A transient and hydrodynamic mathematical model were developed by considering mass, momentum, and energy equations. A finite volume approach was used to solve these governing equations with a structured uniform grid method. According to the results, the micro-channel improved the temperature uniformity of the vapor chamber.

The current study aims to build a compherensive model of the vapor chamber design for the temperature distribution on the wall and pressure and mass flow rate distribution within the wick structure. In this study, interfacial heat transfer coefficient on the liquid-vapor interface for evaporation or condensation processes is calculated. A MATLAB code has been developed to find the vapor temperature via Secant Method. In this code, wick properties such as porosity, permeability, and the working fluid properties are taken into account. The current model is validated with the benchmark study [23] and a parametric study is performed by taking into account the following parameters: heat flux, wick and wall thicknesses, wick and wall thermal conductivity values, ambient temperature, and ambient heat transfer coefficient. According to these findings, the dry-out condition is investigated by comparing the liquid pressure drop and capillary pressure, as well as determining whether the maximum wall temperature exceeds the maximum allowable temperature, which is the maximum operating temperature required for an electronic device to function properly.

1.3 Thesis Structure

Aside from the Chapter 1, Introduction, the current work consists of the following chapters:

Chapter 2: Vapor Chamber Fundamentals: This chapter consists of the fundamental features of vapor chambers. Before analyzing vapor chamber's thermal and flow models, it is important to establish a few key characteristics. Because wick structure is one of the most important aspects of a vapor chamber, it is vital to go over the specifics of the most widely utilized wick types. Permeability which is a wick related parameter is explained. Working fluid type and its compatibility with wick materials are significant selections in terms of fluid properties for the thermal fluid characteristic of vapor chamber, which is why the specifics are described here. Due to how important the vapor chamber's performance limits are, it is important to describe the limits in detail, such as their capillary, boiling, entrainment, and sonic limits.

Chapter 3: Fluid Flow and Heat Transfer Models: This chapter details the fundamental processes that underlie the fluid flow and heat transfer models. The motivation behind this study is discussed at the beginning of this chapter, and then the chapter proceeds to describe in detail the modelling approach that is used to propose a feasible design for a vapor chamber. In addition to that, the assumptions made for the numerical modeling are outlined. Later, the calculation procedure of the temperature, mass flow rate, and pressure distribution is introduced, and in particular, Secant Method is given in depth for the temperature distribution in order to explain how to find vapor temperature. Furthermore, the nodal temperature analysis of the heat source, adiabatic, and heat sink regions includes a detailed description of the mathematical calculation processes that are developed to identify the temperature matrix and to solve the problem of the wall temperature distribution. The MATLAB GUI Vapor Chamber Design Toolbox is created so that all design characteristics of the vapor chamber, such as its size, ambient conditions, and heat flux, could be simply implemented. Following that, the results are calculated and shown in a manner that satisfied the energy, mass, and momentum equations.

Chapter 4: Results and Discussion: The results of the validation study are pre-

sented at the beginning of this chapter. Following that, the temperature distribution and pressure drop of the current study and the benchmark study are compared, and temperature distribution is plotted. Taking into account the fact that the dimensions are the same, parametric research results are presented. These results are obtained by altering various parameters in order to determine the impact that these changes had on the thermal and fluid performance of the vapor chamber, while keeping constant for the remaining parameters. Effect of porosity, wick and wall thicknesses, wall material, different working fluid, and material type couples are investigated in the scope of the parametric study. Based on these results, the condition of dry-out is examined. In addition, in order to meet the requirements for reliable design, the maximum temperature of the system is checked to ensure that it does not go above the maximum temperature that is allowed.

Chapter 5: Conclusion and Future Directions: This chapter is devoted to the analysis and interpretation of the findings presented in Chapter 4. It underlines the significance of the work that was provided in the thesis while also providing a summary of the study that was presented. In addition to that, the contributions that this work has made to the scientific literature are discussed. In conclusion, a conversation is about the potential enhancements that may be made as well as the next steps for this effort. One of the potential enhancements is to carry out an experimental investigation in order to compare the data obtained from experiments with the data obtained from computations. In conclusion, an in-depth discussion on the investigation of a two-phase process is held.

CHAPTER 2

VAPOR CHAMBER FUNDAMENTALS

2.1 Introduction

It is necessary to introduce certain essential parameters before delving into the thermal and hydrodynamic models of the vapor chamber. The following sections will examine the intricacies of the fundamentals, which include the wick structure, the working fluid, the performance constraints, and some significant ideas relating to phase change phenomena.

2.2 Wick Types Used in Vapor Chambers

The wick is a critical component of the vapor chamber because of the capillary action due to its porous medium, which drives the condensed liquid to the heat source zone. A wick structure should be able to hold a sufficient volume of working fluid. Additionally, the thermal properties of the wick have an impact on heat transfer for the processes of conduction, evaporation, and condensation, so the thermo-physical characteristics of the wick material must be good. Wick should exert considerable capillary pressure on the working fluid because the capillary pressure must be greater than the liquid and vapor pressure drop throughout the wick thickness. All properties depend on the wick structure type. Therefore, it is important to investigate the features of each wick type that can be used in vapor chambers. The effect of porosity, the effect of effective thermal conductivity, thermal resistance, permeability, capillary pressure value, and wick material are some of the important parameters of a wick type. These characteristics can help to maximize both the thermal and fluid flow

performance of the vapor chambers. The wick structure governs the heat and mass transfer processes and the overall operation of the vapor chamber. Therefore, further investigation into the wick type should be conducted. The most commonly used wick types in vapor chambers are sintered powder wick, grooved wick, foam wick, and wire mesh wick. Table 2.1 lists the general characteristics of each wick type. Also, the structures of the different types of wicks are demonstrated in Figure 2.1.

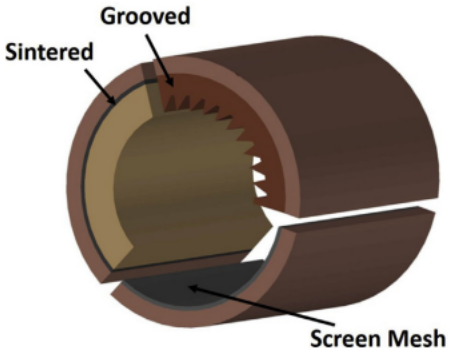

(a) Sintered, grooved and screen mesh wick structures [24]

(b) Foam wick structure [25]

Figure 2.1: Different wick structures

2.2.1 Sintered Wick

Sintered wicks are the most widely utilized wicking structure in vapor chambers. A sintered wick means that the wick is created through the sintering of a chosen material's powder. Typically, the powder is pressed and shaped into a porous medium

at elevated temperatures. It is important that the formed powder must be below the melting point of the material during the sintering process. According to sintering process treatments and sintered wick geometrical features, the properties of sintered wick are affected. During the sintering process, temperature, pressure, and environmental conditions affect the sintered wick properties. In addition to that, sintered wick properties depend on the geometrical parameters of powder such as material, size, and distribution.

2.2.2 Grooved Wick

The parameters of the grooved wick type mostly depend on its material, pattern, and geometry, such as height and width. As shown in the Table 2.1, the grooved type wick has large values for thermal conductivity, porosity, capillary radius, and permeability.

Table 2.1: Wick types and properties [26]

	Sintered	**Grooved**	**Mesh**	**Foam**
Thermal conductivity	Moderate to large effective	Large effective	Small effective	Large effective
Porosity	Small to moderate	Large	Moderate	Large
Capillary radius	Small effective	Large effective	Large effective	Moderate effective
Permeability	Small	Large	Moderate to large	Large

2.2.3 Mesh Wick

Mesh wicks are typically used in heat pipes. The wire diameter and material composition have an effect on the mesh wick's thermal-fluid characteristics. As illustrated in the Table 2.1, this wick has a low effective conductivity, a moderate porosity, a large effective capillary radius, a moderate to high permeability, and a low effective thermal conductivity.

2.2.4 Foam Wick

Foam wicks are made in a variety of ways, including bubbling and deposition. Although foam wicks look similar to sintered wicks, when magnified, they exhibit a distinct structure. As with other wick types, the material and manufacturing process have an effect on the thermal conductivity, porosity, permeability, and capillary radius of the wick.

2.3 Working Fluid Selection and Compatibility with Material

The vapor chamber's performance is influenced by the working fluid chosen. Working fluid must be compatible with the material to prevent vapor chamber damage. Fluid properties like latent heat of vaporization and specific heat capacity are also required to meet the vapor chamber's thermal-fluid performance requirements. Depending on the application, the working fluid should be chosen. Water, ethanol, methanol, acetone, ammonia, and pentane are some of the fluids that are utilized in heat pipes and vapor chambers. Aside from the type of working fluid, the filling ratio has an impact on thermal performance.

Lu et al. designed a vapor chamber, and conducted experiments using graphite foam as the wick material and ethanol as the working fluid [27]. The authors of this study examined the effects of several constraints on the thermal performance of the vapor chamber, including the capillary limit, the boiling limit, and thermal resistance. Different ethanol filling ratios were evaluated, and the optimal ratio was determined. Additionally, water was employed as the working fluid, and the results indicated that performance was approximately twice as good when water was used instead of ethanol. Chen et al. compared the performance of VCs with radial grooved wicks to that of sintered powder wicks [28]. Aluminum was used for the wick material, and acetone was used as the working fluid. The results showed that the filling ratio of working fluid affected the overall performance of the vapor chamber for both wick types. Because of that, the optimum charging ratio was found by testing different heat inputs. In contrast to the radial grooved VC, whose performance depended on how much heat was put into it, the overall thermal resistance of the sintered wick VC

was the same across the range of heat inputs that were tested. Ji et al. carried out the design and testing procedures for a vapor chamber with a copper foam wick structure [29]. Three types of working fluids (acetone, water, and ethanol) were evaluated in this investigation. The vapor chambers that used water as their working fluid had the best thermal performance out of the three used in the studies. The vapor chambers that used ethanol as their working fluid had the worst thermal performance. Also, the thermal performance of vapor chambers was affected by how much they were filled and how they were tilted. The vapor chamber, which used water as a working fluid, had the lowest thermal resistance and a maximum heat load of 170 W. This limit was put in place to make sure that the capillary and boiling limits were not exceeded. The studies on vapor chamber performance were carried out by Wong et al. who used water, methanol, and acetone as working fluids [30]. The wick was made up of two layers of sintered mesh. Water had the lowest resistance in a vapor chamber because its latent heat value is higher than that of acetone. This means that a vapor chamber with water as the working fluid can handle a higher heat load value. The researchers also looked at how the size of the heat source impacted thermal performance. They found that for all three fluids, spreading resistances were higher when the heat source was smaller.

The heat is transferred through two-phase phenomena in vapor chambers. A working fluid saturated with both liquid and vapor present in the vapor chamber is required for a vapor chamber to function. On the heat source side, the vapor chamber absorbs heat from a heat source to evaporate, and on the heat sink side, the vapor chamber releases its latent heat for condensation. In addition, the vapor chamber potentially works somewhere between the triple point and the critical point. The triple point is where all three phases, solid, liquid, and gas, are in equilibrium and have their own temperature and pressure values. The liquid–vapor critical point, which is the point on the pressure–temperature curve where a liquid and its vapor may coexist, is the most well-known example.

As a result, the working fluid parameters such as triple point, critical point, and latent heat value at a variety of temperatures are necessary for the effective operation of a vapor chamber. The temperature range for each vapor chamber application is different. The vapor chamber can be filled with a variety of working fluids depending

on the application to enhance heat transfer capacity and minimize thermal resistance. Hence, the vapor chamber must provide the proper working fluid while considering the needed temperature range. Similarly, depending on their intended application, the vapor chambers' containers can be composed of a variety of materials. In the selection process, the compatibility of the vapor chamber containment material with the working fluid is critical. If any of the components, such as the wick, container, or working fluids, are incompatible, the vapor chamber's performance may be harmed, and failures may occur. Wick material and working fluid have some applications in the industry. For electronic cooling, the most popular container material-working fluid couples are copper-water and copper-methanol. While water, the most commonly used working fluid, has good thermophysical properties including a high heat of vaporization and low surface tension, it also has the added benefit of being fully safe to handle while in use. Aluminum, on the other hand, is commonly utilized with ammonia as a working fluid in space applications due to its lightweight structure. Higher surface tension, latent heat of vaporization, and thermal conductivities are required for higher temperature applications, hence superalloy-alkali metals with a wide working temperature range are used. According to experimental compatibility testing, the working fluid and its compatible material types are listed in Table 2.2.

Table 2.2: Working fluids and compatible materials [31]

Working fluid	**Compatible material(s)**
Water	Stainless Steel, Copper, Silica, Nickel, Titanium
Ammonia	Aluminum, Stainless Steel, Iron, Cold Rolled Steeled, Nickel
Methanol	Stainless Steel, Iron, Copper, Brass, Silica, Nickel
Acetone	Aluminum, Stainless Steel, Copper, Brass, Silica
Freon-11	Aluminum
Freon-21	Aluminum, Iron
Freon-113	Aluminum
Heptane	Aluminum
Dowtherm	Stainless Steel, Copper, Silica
Lithium	Tungsten, Tantalum, Molybdenum, Niobium
Sodium	Stainless Steel, Nickel, Niobium
Cesium	Titanium, Niobium, Stainless Steel, Nickel-based superalloys
Mercury	Stainless Steel
Lead	Tungsten, Tantalum
Silver	Tungsten, Tantalum

Corrosion, non-condensable gas production, and materials transfer are examples of issues that might develop when incompatible fluid/envelope pairings are utilized. Non-condensable gas generation is caused by impurities or pollutants in the working fluid on the wick or wall. When the working fluid is incompatible with the wall or wick material, corrosion occurs. Corrosion products might clog a section of the wick, reducing the maximum power. In more severe cases, a leak can develop, making the vapor chamber inoperable. Material transportation is another issue that can develop in a vapor chamber. If the working fluid contains a chemical that is highly soluble in one or more of the components of the wick or envelope, some dissolved components can impede the flow transit path during evaporation and condensation processes. Because of these issues, the appropriate tests for compatibility between the working fluid and the wick structure must be undertaken before the vapor chamber is designed and manufactured.

2.4 Effective Wick Thermal Conductivity Calculation

Within the wick structure, conduction processes are typically the predominant mechanism that are present. Although there is some fluid motion within this layer as a result of the circulation of working fluid, convection effects within the wick are typically ignored because the liquid velocity within the wick is very low. This is because the circulation of working fluid causes some fluid motion within this layer. The liquid velocity in the wick is typically estimated to be on the order of 0.5-1 mm/s [26, 32]. Therefore, considering convective mechanisms irrelevant in VC operation due to the extremely low liquid velocity seen within the wick zone during VC operation. Wick has a porous medium and the porosity is denoted by ε. Porosity can be expressed as a function of volume occupied solid and fluid. It is shown in Equation 2.1 where V_l is the volume occupied by the working fluid and V_s is the volume of the solid part of the wick $V_l + V_s$ is the total volume of the wick. Therefore, to calculate the thermal conductivity of the wick, the solid and liquid parts should be taken into consideration and it is called effective thermal conductivity of the wick. So, the effective thermal conductivity of the wick region is also a very important metric of how well a two-phase device works. A high value for this parameter indicates that the wick has a small temperature drop, which improves thermal performance.

$$\varepsilon = \frac{V_l}{V_l + V_s} \tag{2.1}$$

In this thesis, sintered sphere wick as a wick type is used for the parametric study, so in literature [33–35], the effective thermal conductivity can be determined using the Equation 2.2 shown.

$$k_{eff} = \frac{k_l((k_l + k_s) - (1 - \varepsilon)(k_l - k_s))}{(k_l + k_s) + (1 - \varepsilon)(k_l - k_s)} \tag{2.2}$$

2.5 Permeability Calculation of the Wick Structure

Permeability is an important property for the wick structure, because permeability is related to the ability of the working fluid to pass through the wick structure. This means that the permeability is linked to the liquid pressure drop within the vapor chamber. When the working fluid travels through the wick structure, as it must in order to return to the heat source zone due to the liquid pressure loss. Liquid pressure drop can be described in the Equation 2.3 for a heat pipe with a simple shape [36].

$$\Delta P_l = \frac{\mu_l L \dot{m}_l}{\rho_l K A_w} \tag{2.3}$$

Equation 2.3 shows that larger permeability causes small pressure drop within the vapor chamber [37]. In order to have a small drop in liquid pressure and, therefore, a better ability to move heat, the permeability needs to be large. Most of the time, permeability depends on the geometric dimensions of the wick type. As previously mentioned, permeability values change according to wick type, and these values are calculated according to experiments. Giraudon et al. [38] studied the effects of the characteristics of porous wicks. This study showed that the manufacturing procedure, which included obtaining different porous samples, affect the permeability values of the wick structure. It was also concluded that having a high permeability is a critical factor in achieving optimum thermal performance. Additionally, in the literature, according to experimental permeability values, the permeability equations that depend on the wick properties such as pore radius and porosity can be obtained. As shown in Equation 2.4, the permeability of a wick structure with an array of channels with circular cross section pores was calculated [36].

$$K = C\frac{d_p^2 \varepsilon}{32} \tag{2.4}$$

C coefficient depends on the flow type. If it was assumed as Hagen-Poiseuille flow, then it would equal 1. Additionally, if the permeability test was performed for sintered metal powders, Equation 2.5 which was also called as the Chi Equation can be written as follows:

$$K = \frac{r_p^2 \varepsilon^3}{37.5(1-\varepsilon)^2} \tag{2.5}$$

Equation 2.5 is also known as the Blake-Kozeny equation [39,40]. In addition to that, Williams and Harris determined the correlations between the pore size and permeability using capillary flow porometry and pressure-flow rate data [41]. Holley and Faghri performed the rate-of-rise test measurements to determine the methods for permeability and effective pore radius values [42]. In this thesis, Equation 2.5 is used for permability to calculate the liquid pressure distribution within the system which is explained in Section 3.1.3.

2.6 Vapor Chamber Performance Limits

The temperature drop is related to the variation of the pressure for both liquid and vapor inside the heat pipe. Operating temperature of the working liquid is crucial in terms of properties of both liquid and wick type. Some properties should be concerned to design a two-phase cooling device: In terms of service life, the selection of wick and wall materials should be compatible; otherwise, failure or corrosion can happen, which causes a decrease in performance. Vapor pressures must not be too high or too low for the operation range. As mentioned in previous sections, there should be enough driving force to circulate the working fluid inside the wick structure. The capillary action of the wick structure is crucial because the total pressure drop must be lower than the maximum capillary pressure to work under reliable conditions. In general, Equation 2.6 shows this condition [37]. This circumstance, which is also known as a capillary limit, is critical for the wick structure to function properly. Dry-out at the wick will occur if the heat load creates a liquid pressure drop that is greater than the capillary pressure head. The capillary limit refers to the threshold heat flux that must be exceeded in order to dry-out the wick. This happens when the capillary pumping is not sufficient to carry enough liquid from the heat sink region to the heat source region. Due to the effects of dry-out, the thermodynamic cycle is unable to continue, and the vapor chamber is no longer operating as it should. As a result, it is essential to calculate the dry-out heat flux value, which is the highest value that enables the vapor chamber to perform its desired functionality.

$$\Delta P_c \geq \Delta P_l + \Delta P_v + \Delta P_{gr} \tag{2.6}$$

Other limitations for the transportation of liquid and vapor are the boiling limit, entrainment limit, and sonic limit. Boiling occurs when the heat flux exceeds the critical heat flux (CHF) limit and causes nucleate boiling as well as bubbles. They block the liquid from flowing throughout the evaporator section. The entrainment limit occurs due to high vapor velocity at lower temperatures. When the temperature decreases, the vapor pressure and density also decrease. This causes disconnections of liquid droplets and entrained in the vapor. Another limitation is the sonic limit that vapor velocity reach [37]. Lower vapor temperature values cause lower vapor pressure; therefore, the vapor velocity increases in order to carry a given amount of heat, and the compressibility effects of the vapor are observed. In this limitation, more pressure difference is not be able to increase the flow velocity because of the reaching sonic limitation.

CHAPTER 3

FLUID FLOW AND HEAT TRANSFER MODELS

In this study, the potential improvement has been performed to increase the heat spreading and heat removal capacities for high heat flux devices. To do that, an effective vapor chamber modelling is developed. This design modelling helps to investigate the design needs for high-powered electronic components. To model the vapor chamber, a code is developed and for this purpose, MATLAB is used to find all thermal-fluid properties according to given design parameters such as size of the VC, coolant properties, etc.. As shown in the Figure 3.1a, the vapor chamber is divided into three regions: heat source, adiabatic, and heat sink. Heat source region is where power is given from the heat source, adiabatic region is where the heat transfer does not occur with exterior and heat sink region is where the heat is dissipated. In the calculations, the half vapor chamber is considered and divided at the line of symmetry to ease the modeling and calculate the parameter distributions. In this model, to satisfy the continuity equation, the evaporated mass flow rate must be equal to the condensed mass flow rate. Therefore, it is assumed that as shown in Figure 3.1b, at points, $x = 0$ and $x = L_{hs} + L_{adia} + L_{hsi} = L_{total}$, mass flow rate of the working fluid must be equal to zero. The vapor phase turns to the liquid phase inside the wick by releasing latent heat because the vapor temperature is higher than the wall temperature and condensation occurs. The condensation process continues until the point where the wall temperature is lower than the vapor temperature. At this point, the wall temperature starts becoming higher than the vapor temperature and the evaporation process starts and this continues until the line of symmetry $x = 0$ on the heat source side which the liquid mass flow rate of the working fluid becomes zero. This is only one circulation of the working fluid throughout the wick structure.

Another important point is to find the operating vapor temperature according to given design parameters. Vapor temperature is found via Secant Method. To do this, the vapor chamber is discretized into the elements to make the comparison in each node. The purpose of finding the vapor temperature is to determine whether the evaporation or condensation process occurs at each node. After the vapor temperature value is found and then, this value is compared to wall temperature. If the vapor temperature is higher than the node wall temperature, working fluid condenses, otherwise, the working fluid evaporates. This comparison is done at each node of the VC element. To make clear of this process, the calculation algorithm flow chart is shown in Figure 3.2. All calculations are done iteratively in the code. Also, this process shows that in addition to the case which evaporated and condensed mass flow rates are equal, dry-out condition must be satisfied in order for vapor chamber to work properly. MATLAB code calculates the dry-out condition by calculating and comparing the capillary pressure head and liquid pressure drop. If the liquid pressure drop in the system is lower than capillary pressure head, the vapor chamber design works properly, otherwise, there is no possible solution with given operating conditions.

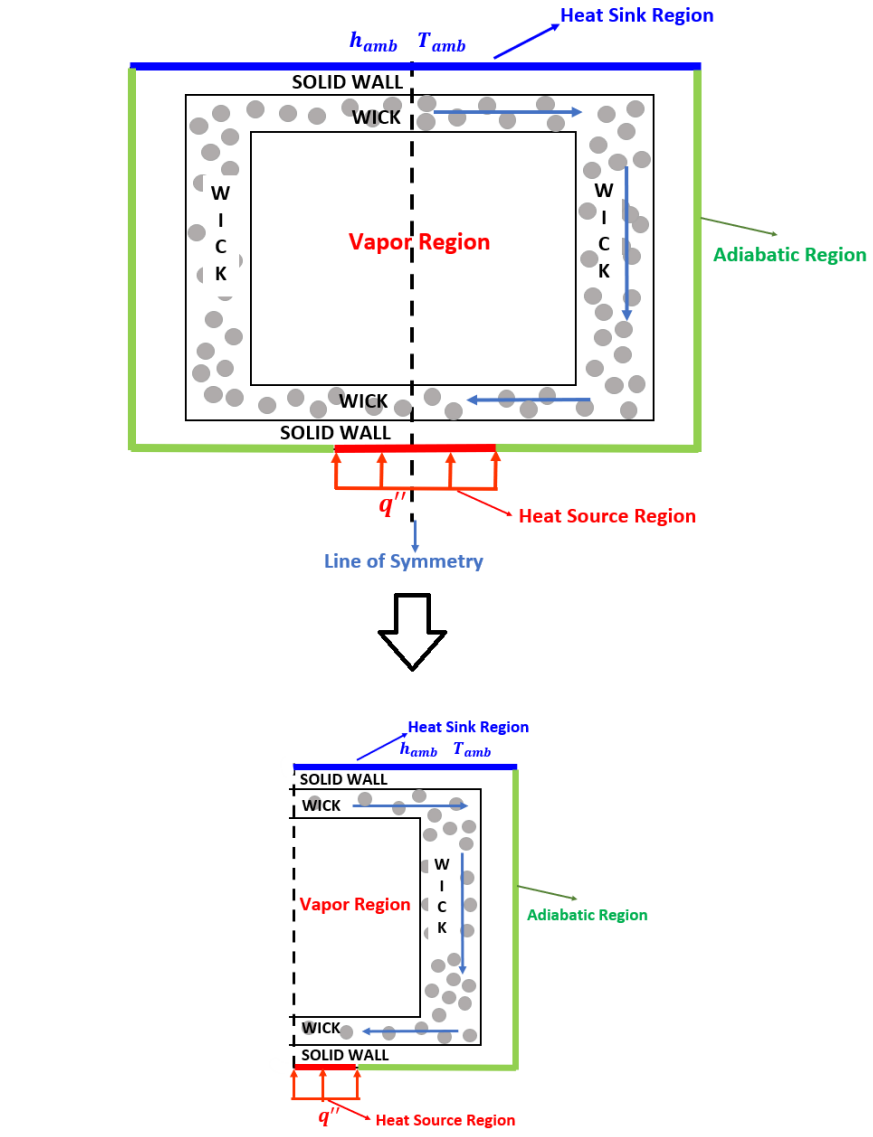

(a)

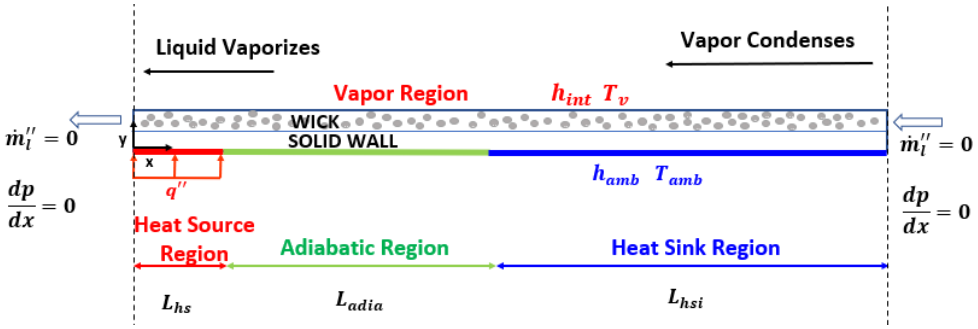

(b)

Figure 3.1: Schematic diagram of the vapor chamber

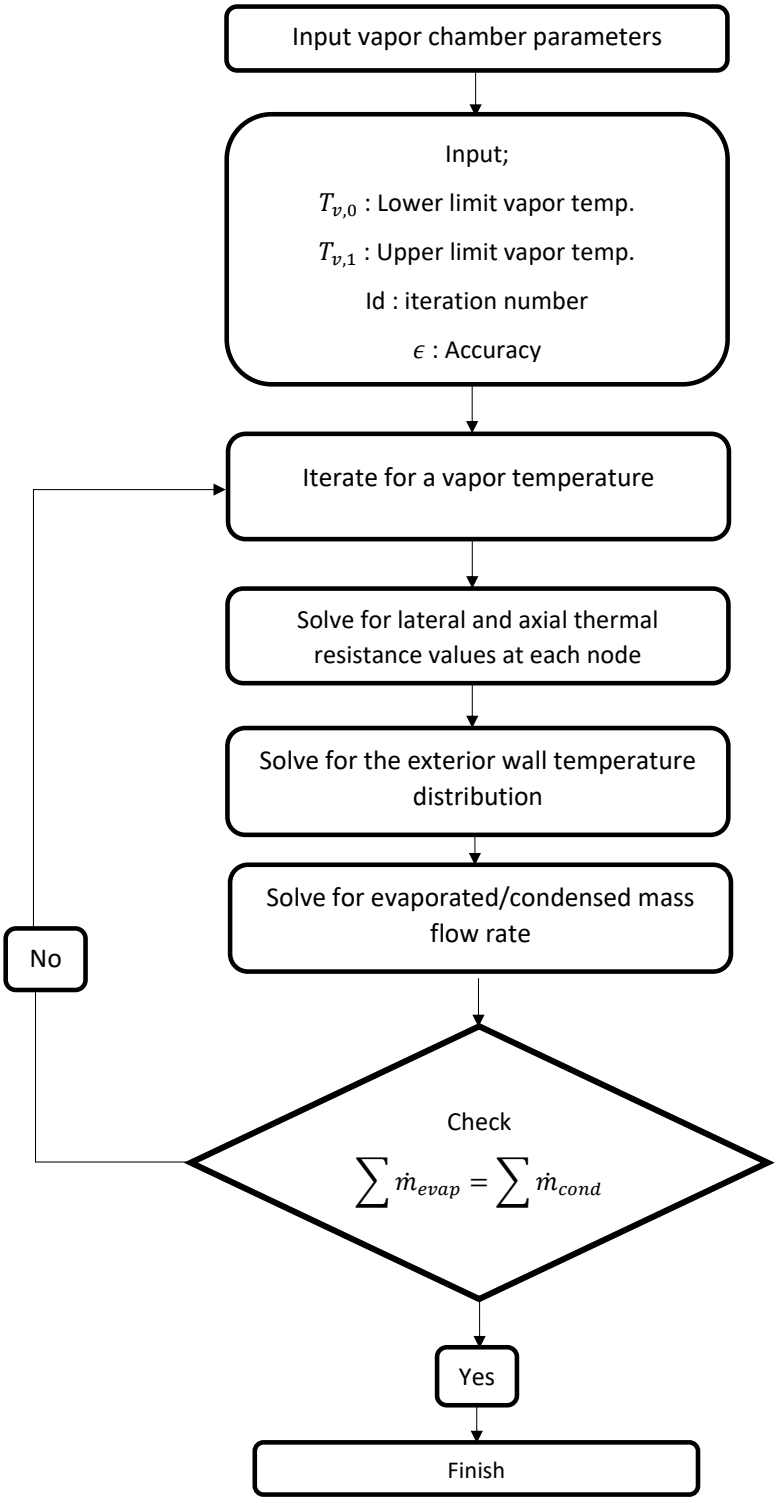

Figure 3.2: Flow chart of the process

In the following sections, detailed information of the numerical calculation procedure of the thermal and fluid properties for the VC will be given. Before that it is important to mention the assumptions used in the model.

1. Fluid flow in wick is assumed to be laminar.
2. Fluid flow in wick is assumed to be incompressible.
3. All processes are time-independent
4. Saturation condition is only assumed at the liquid vapor interface.
5. Sintered sphere wick mesh type wick structure is used.
6. Two-dimensional cartesian coordinate system is used for modeling.

3.1 Modelling Approach

In the scope of the numerical model of the vapor chamber, the goal is the calculation of the wall temperature distribution, the mass flow rate, and the pressure variation throughout the wick structure by taking into consideration the design parameters of the vapor chamber such as heat source lengths, size of the VC, wall and wick thicknesses including wick parameters such as porosity, permeability, etc. and the heat sink side ambient conditions (heat transfer coefficient and ambient temperature). The current modeling approach is carried out in two-dimensional. The generalized governing equations of the mass, momentum and energy in the two phases and the liquid/vapor interface as well as the conduction equation in the solid walls, as follows:

The continuity equation for the wick:

$$\dot{m}_{in} + \frac{\partial(\rho u)}{\partial x} dx = \dot{m}_{out} \tag{3.1}$$

The two-dimensional momentum equations in the wick are:

$$\frac{\partial \rho u}{\partial t} + \nabla \cdot (\rho \overrightarrow{V} u) = \frac{\partial \varepsilon P}{\partial x} + \nabla \cdot (\mu \nabla u) - \frac{\mu \varepsilon u}{K} \tag{3.2}$$

$$\frac{\partial \rho v}{\partial t} + \nabla \cdot (\rho \overrightarrow{V} v) = \frac{\partial \varepsilon P}{\partial x} + \nabla \cdot (\mu \nabla v) - \frac{\mu \varepsilon v}{K} \tag{3.3}$$

The energy equation in the wall and wick is:

$$\frac{\partial}{\partial x}(k\frac{\partial T}{\partial x}) + \frac{\partial}{\partial y}(k\frac{\partial T}{\partial y}) + \dot{q} = \rho c_p \frac{\partial T}{\partial t} \tag{3.4}$$

This can be done with discretization of three main regions of the vapor chamber which are heat source, adiabatic, and heat sink. It is important to mention that the half of the vapor chamber in other words, line of symmetry is taken into consideration for all calculation steps. This means that half length of the heat source and heat sink region is used. To calculate the temperature, mass flow rate and pressure distributions, these sections are discretized as Δx. The general discretized model is shown in Figure 3.3. In addition to that wick and solid wall thickness and thermal conductivity are shown in Figure 3.4. k_w and k_b are the thermal conductivity values of wick and solid wall, respectively. Also, y_w and y_b are the thickness values of wick and solid wall, respectively.

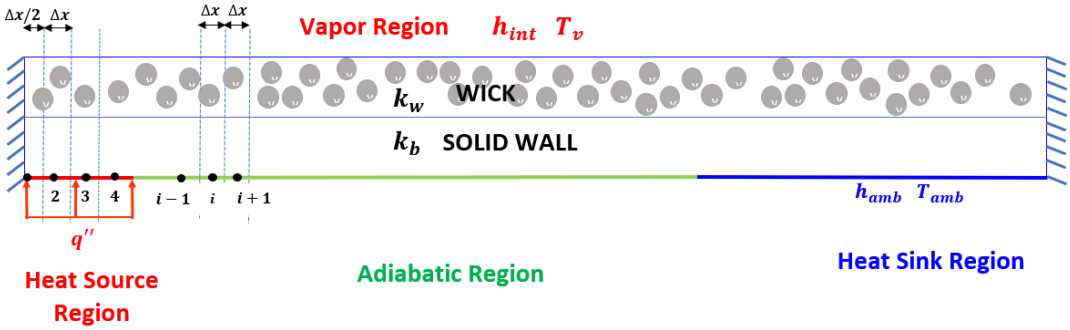

Figure 3.3: Discretized model

3.1.1 Wall Temperature Distribution Calculation

In this section, the details to calculate the temperature distribution on the outside wall of the vapor chamber is presented. As shown in Figure 3.4, after discretization of the VC, the amount of heat entering and leaving are determined at each node of the control volume via conduction, convection and phase-change. Figure 3.5 shows the nodal analysis of the each region on the vapor chamber. Lateral and axial thermal resistance values are calculated in the following Equations 3.6 and 3.8, respectively.

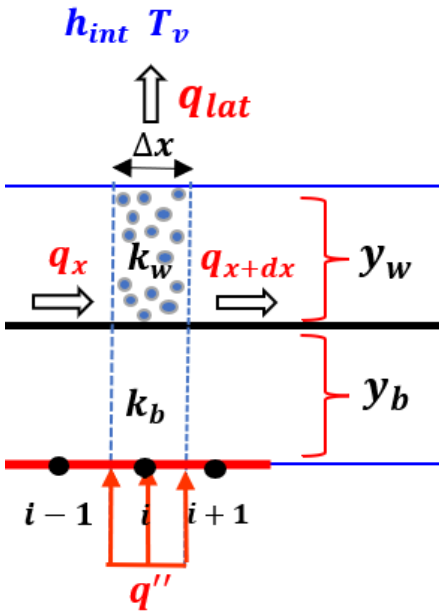

Figure 3.4: Energy balance on a discrete element

Both thermal resistances in lateral and axial directions include the thermal conductivity and the thickness values of the wall and wick. As distinct from axial thermal resistance, lateral thermal resistance includes heat transfer coefficient on the liquid-vapor interface which is used to find the evaporated or condensed mass flow rate on the liquid-vapor interface by Kinetic Theory. In two-phase cooling devices, another important point is the phase change mechanisms for evaporation and condensation. Accordingly, evaporative or condensive mass flux can be calculated based on the interfacial properties of the vapor and liquid. At near equilibrium conditions, when the evaporation or condensation rate is not exccessive. Equation 3.5 is used to calculate interface heat transfer coefficient [26].

$$h_{int} = \left(\frac{\hat{\sigma}}{1-\hat{\sigma}}\right)\left(\frac{\rho_v h_{fg}^2}{T_v}\right)\left(\frac{M}{2\pi R_u T_v}\right)^{1/2}\left(1-\frac{P_v}{2\rho_v h_{fg}}\right) \tag{3.5}$$

In addition, for the calculation heat transferred value in lateral direction depends on the difference between the wall node temperature and vapor temperature values. Conservation of mass states that evaporated and condensed mass flow rates must be equal so, the appropriate vapor temperature value which satisfies the continuity is determined by Secant Method. According to the vapor temperature, the difference between

the vapor temperature and wall temperature at each node, used to whether evaporation or condensation occurs. If the wall temperature is greater than vapor temperature, the working fluid evaporates, otherwise, it condenses.

To determine the wall temperature distribution, lateral and axial thermal resistances are calculated as shown in Equations 3.6, 3.7 and 3.8. In order to calculate the lateral thermal resistance, there are two conditions: While Equation 3.6 is used in the heat source and adiabatic regions, Equation 3.7 is used in the heat sink region because there is a heat transfer between ambient side. Figure 3.5 shows the nodal points of the each region on the vapor chamber. On each node, temperature-dependent equations are written, and this set of equations forms a matrix. The wall temperature distribution is obtained by solving the systems of linear equations.

$$R_{lat} = \frac{y_w}{k_w \Delta x} + \frac{y_b}{k_b \Delta x} + \frac{1}{h_{int} \Delta x} \tag{3.6}$$

$$R_{lat} = \frac{y_w}{k_w \Delta x} + \frac{y_b}{k_b \Delta x} + \frac{1}{h_{int} \Delta x} + \frac{1}{h_{amb} \Delta x} \tag{3.7}$$

$$R_{ax} = \frac{R_w R_b}{R_w + R_b} \qquad \text{where} \qquad R_w = \frac{\Delta x}{k_w y_w} \quad , \quad R_b = \frac{\Delta x}{k_b y_b} \tag{3.8}$$

Generalized equation to calculate the nodal wall temperature of each region is shown in Equation 3.9. The important point is that the heat flux term in this equation disappears for the equations in the adiabatic and heat sink regions.

$$T_{i-1}\left(\frac{1}{R_{ax}} + \frac{1}{R_{lat}}\right) - T_i\left(\frac{1}{R_{ax}}\right) + T_{i+1}\left(\frac{1}{R_{ax}}\right) = q^{''}\Delta x + \frac{T_v}{R_{lat}} \tag{3.9}$$

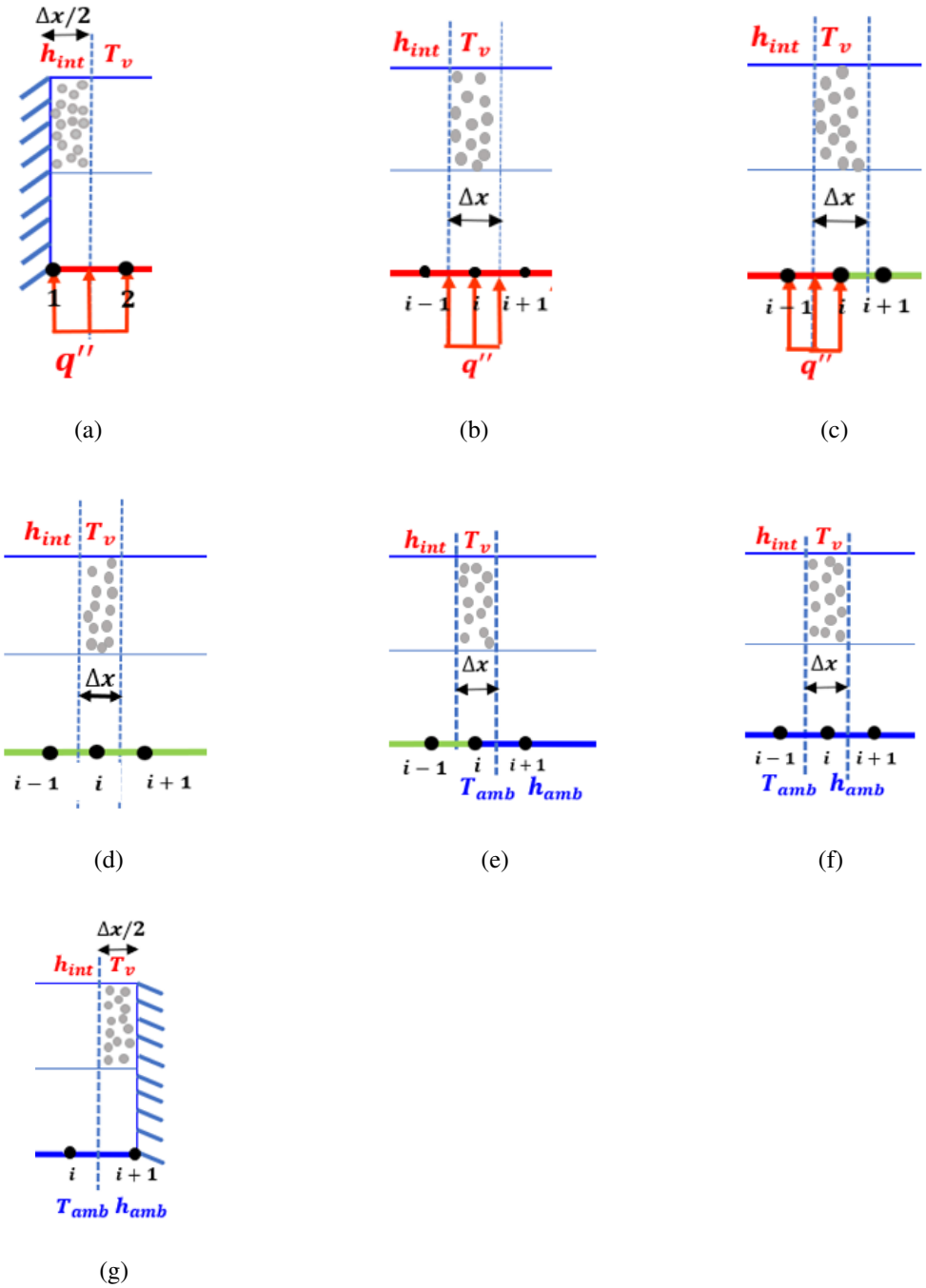

Figure 3.5: Nodal analysis of the each region on the vapor chamber model

3.1.2 Mass Balance Calculations

After finding the vapor temperature and wall temperature distribution, evaporated or condensed mass flow rate can be calculated. Evaporation or condensation is determined according to difference between the vapor temperature and wall temperature. If the wall temperature is greater than the vapor temperature evaporation occurs, if the wall temperature is less than the vapor temperature condensation occurs. This condition is checked at each node. In addition, the lateral heat transfer leads to phase change process. Evaporated or condensed heat flow rate is calculated as follows:

$$q_{lat} = \frac{T_b - T_v}{R_{lat}} \tag{3.10}$$

Evaporated or condensed mass flow rate is calculated as follows:

$$\dot{m}_{evap/cond} = \frac{q_{lat}}{h_{fg}} \tag{3.11}$$

Evaporated or condensed mass flux is calculated as follows in Figure 3.6:

$$\dot{m}''_{out} y_w = \dot{m}''_{in} y_w \pm \dot{m}''_{evap/cond} \Delta x \tag{3.12}$$

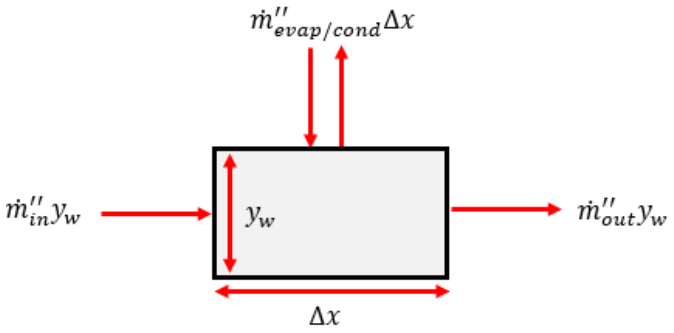

Figure 3.6: Mass balance on the discrete element

3.1.3 Pressure Distribution Calculation

Pressure calculation is a crucial step in this model because according to pressure drop throughout the wick structure, it is checked if there is enough driving force for the working fluid to circulate inside the wick. The capillary pressure value is used to control this. If the difference between maximum and minimum pressure value is greater than capillary pressure, dry-out condition occurs, and the working fluid cannot circulate. This is not an intended situation, so vapor chamber must be designed so that the difference between the maximum and minimum pressure value must be less than capillary pressure. In this model, it is assumed that pressure variation of the working fluid is considered only along the x-axis. Force balance of the control volume as shown in the Figure 3.7 where y_w is the wick thickness, τ_w is the shear stress on the wick.

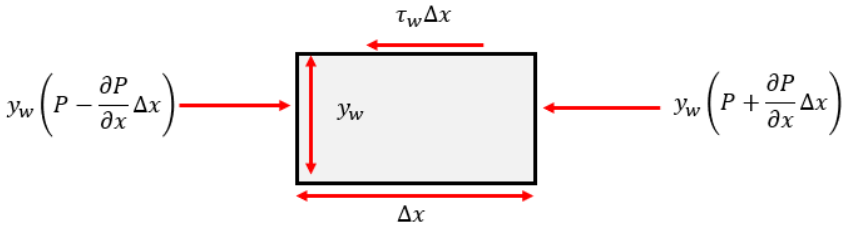

Figure 3.7: Force balance of the control volume

$$y_w(P - \frac{\partial P}{\partial x})\Delta x - y_w(P + \frac{\partial P}{\partial x})\Delta x + \tau_w \Delta x = 0 \tag{3.13}$$

$$\frac{\partial P}{\partial x} = \frac{dP}{dx} = \frac{\tau_w}{y_w} \tag{3.14}$$

Friction factor can be defined as follows [43]:

$$f = \frac{\tau_w}{\rho u^2/2} \tag{3.15}$$

Reynolds number can be defined as follows:

$$Re = \frac{\rho u y_w}{\mu} \tag{3.16}$$

Permeability of the wick, can be defined as follows [33]:

$$K = \frac{y_w^2}{2fRe} \tag{3.17}$$

Multiplying and dividing Equation 3.15 by velocity, u

$$\rho u^2 = \frac{uRe\mu}{y_w} \tag{3.18}$$

Combining Equations 3.15 and 3.18, wall shear stress becomes

$$\tau_w = \frac{fuRe\mu}{2y_w} \tag{3.19}$$

Equation 3.14 becomes

$$\frac{dP}{dx} = -\frac{f\rho u^2/2}{y_w} = -\frac{fuRe\mu}{2y_w^2} = -\frac{u\mu}{K} \tag{3.20}$$

Finally, pressure drop on a discretized element can be expressed as a function of the permeability of the wick structure.

$$\frac{dP}{dx} = -\frac{u\mu}{K} \tag{3.21}$$

In order to find pressure distribution within the wick, the pressure value at each node is calculated as follows:

$$P_{i+1} = P_i - \Delta x \frac{u\mu}{K} \tag{3.22}$$

3.1.4 Dry-out considerations

As mentioned in Section 2.6, the maximum amount of heat load that can be maintained in a steady state is determined by the equilibrium between the capillary pressure that is provided by the wick in a vapor chamber and the flow resistance to liquid resupply. As stated in Equation 3.21, liquid pressure drop depends on the wick and working fluid properties. In the same way, the capillary pressure can be stated in the form of an Equation 3.23, capillary pressure depends on the surface tension σ, capillary radius r, and contact angle θ. Figure 3.8 shows that surface tension for different working fluid types is a temperature dependent parameter. Increasing the given heat load causes a decrease in capillary pressure due to the temperature increasing in the system; conversely, increasing the heat flux causes an increase in the liquid pressure drop in the system due to the increasing liquid velocity. Using different working fluids and wick structures affects both capillary pressure and liquid pressure drop in the system. Therefore, it is important to investigate and discuss different case studies. In this thesis, the dry-out condition is taken into consideration in the parametric study to show the maximum heat load, also called dry-out heat flux, which the system is able to carry out without dry-out.

$$\Delta P_c = \frac{2\sigma}{r}\cos\theta \tag{3.23}$$

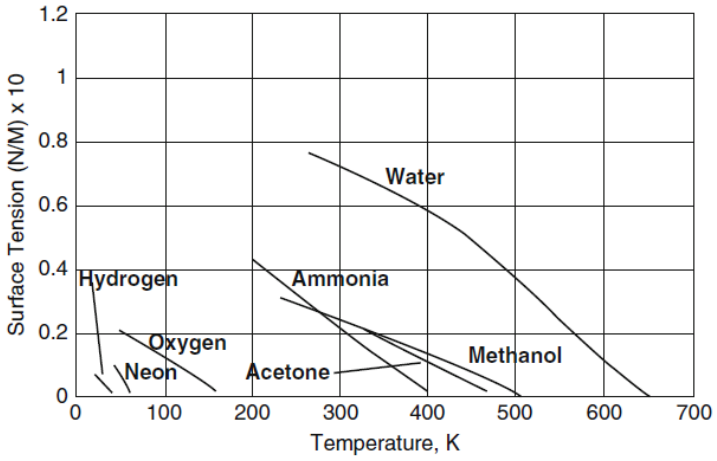

Figure 3.8: Surface tension for different working fluid types [44]

3.2 Numerical Model Implementation to MATLAB

As demonstrated in Figure 3.9, a vapor chamber design toolbox is developed using the MATLAB GUI. This toolbox enables the input of the design parameters and simulation performance. After obtaining the temperature distribution on the wall, the pressure distribution, and the mass flow rate distribution across the vapor chamber, the corresponding example graphs are drawn as shown in Figure 3.10, Figure 3.11 and Figure 3.12. The temperature distribution in Figure 3.10 illustrates the vapor temperature determined using Secant Method described in the preceding section. In addition, when the wall temperature equals the vapor temperature, the phase change process changes from evaporation to condensation, or vice versa. Evaporated and condensed mass flow rates are shown to be equivalent in the mass flow rate distribution Figure 3.11, demonstrating that the continuity equation is satisfied.

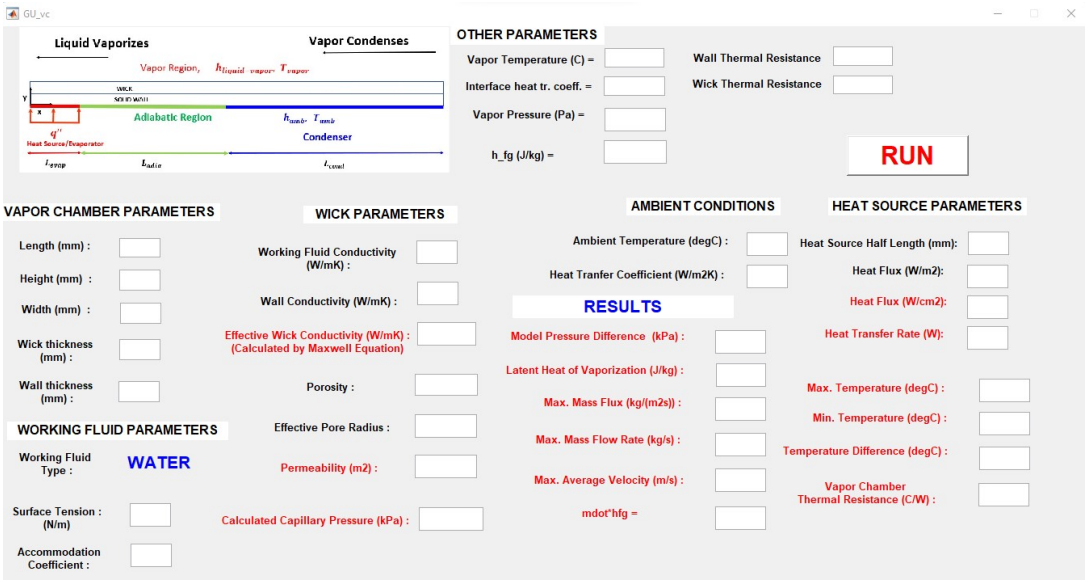

Figure 3.9: Graphical user interface vapor chamber toolbox

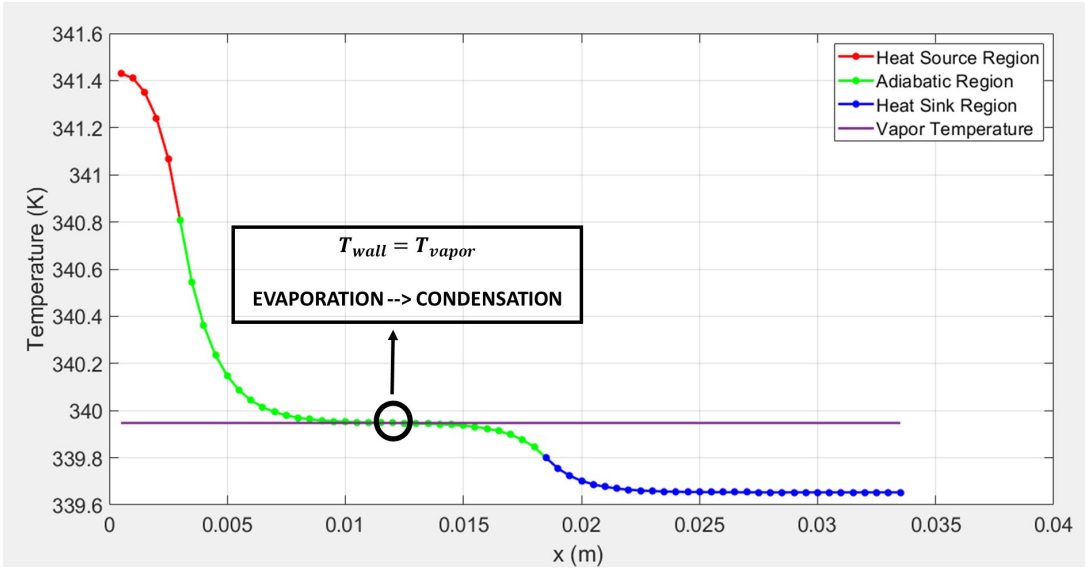

Figure 3.10: Wall temperature distribution example plot

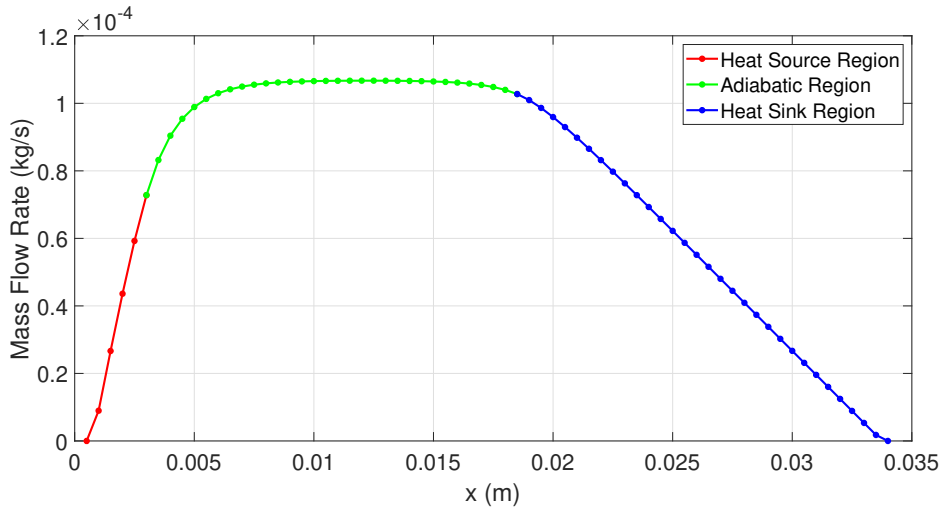

Figure 3.11: Mass flow rate plot

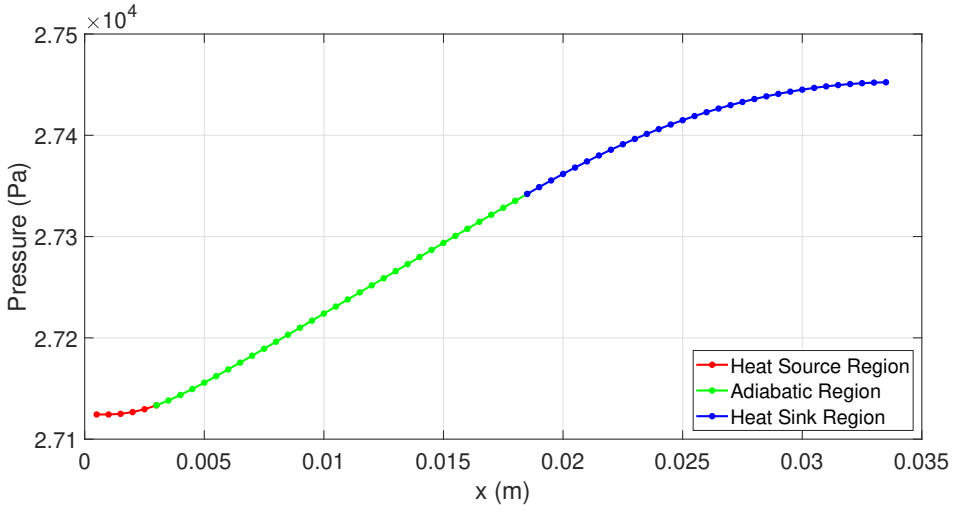

Figure 3.12: Pressure distribution plot

CHAPTER 4

RESULTS AND DISCUSSION

4.1 Verification Study

To ensure the validity of the vapor chamber model, the same wick properties and boundary conditions as in the study of Ranjan et al. [23] is used and the results are compared. Comparison is made according to the results of the benchmark study. In the benchmark study [23], a two-dimensional vapor chamber model, also called the device-level model, is numerically solved using ANSYS Fluent. Continuity, momentum, and energy equations for each region of the vapor chamber are solved. In Fluent, user defined functions (UDFs) have been made to figure out the mass flow rates of evaporation and condensation as well as the temperature and pressure at the wick-vapor interface. Also, Brinkman- Forchheimer extended Darcy model is used to analyze the flow of the liquid through the wick. The details of the device model in the benchmark study are shown in Figure 4.1. Also, Table 4.1 shows the physical dimensions, wick and wall properties, and operating parameters of the VC.

As shown in Figure 4.1, there are three zones: heat source, heat sink, and adiabatic. Water is used as the working fluid, and the material of the wall is copper. A screen mesh type is used for the wick structure. Note that, in the benchmark study, two different accommodation coefficient values are used. According to previous studies, the range of accommodation coefficient changes between 0.028 and 1 [45, 46]. Also, thermal performance substantially affects the value of the accommodation coefficient. Therefore, the values 0.03 and 1 are used in the benchmark study to see the effect on thermal performance of the vapor chambers.

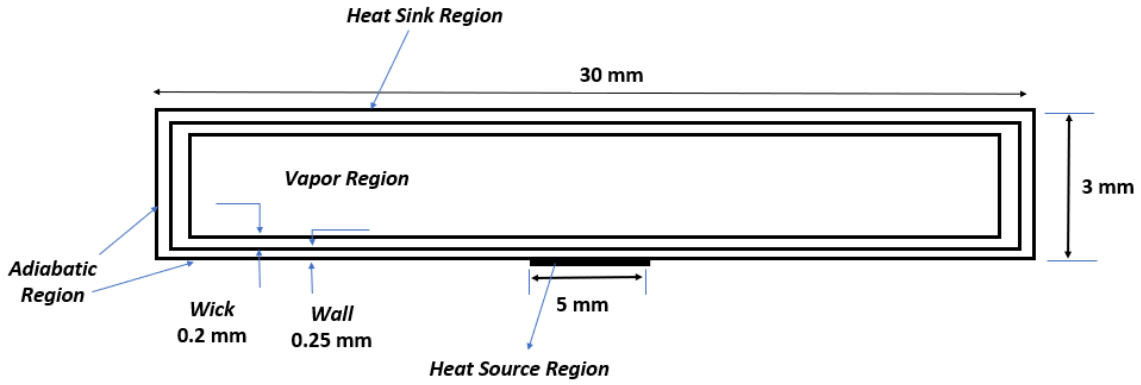

Figure 4.1: Schematic diagram of the vapor chamber model in the benchmark study, adapted from [23].

Table 4.1: Benchmark model [23] vapor chamber dimensions, wick and wall properties and operating parameters

Parameter	**Value**
Length (mm)	30
Height (mm)	3
Heat source size (mm)	5
Wall thickness (mm)	0.25
Wick thickness (mm)	0.2
Wick type	Sintered screen mesh
Wick thermal conductivity $(\mathrm{W}/(\mathrm{m}\cdot\mathrm{K})$)	40
Wick permeability (m^2)	2.97×10^{-11}
Wick porosity	0.56
Material type	Copper
Wall thermal conductivity $(\mathrm{W}/(\mathrm{m}\cdot\mathrm{K})$)	387.6
Working fluid type	Water
Accommodation coefficient	0.03 and 1
Heat flux $(\mathrm{W}/\mathrm{cm}^2)$	10
Coolant water temperature (K)	298
Heat transfer coefficient $(\mathrm{W}/(\mathrm{m}^2\cdot\mathrm{K}))$	400

4.1.1 Comparison of the Current and Benchmark Studies

To validate the current vapor chamber modeling, the same boundary conditions and thermophysical properties are applied. In the benchmark study, the heat flow rate is 500 W. In the current study, half of this value is applied because the current modeling approach uses the half size of the vapor chamber due to symmetry since the half size of the heat source region is 2.5 mm.

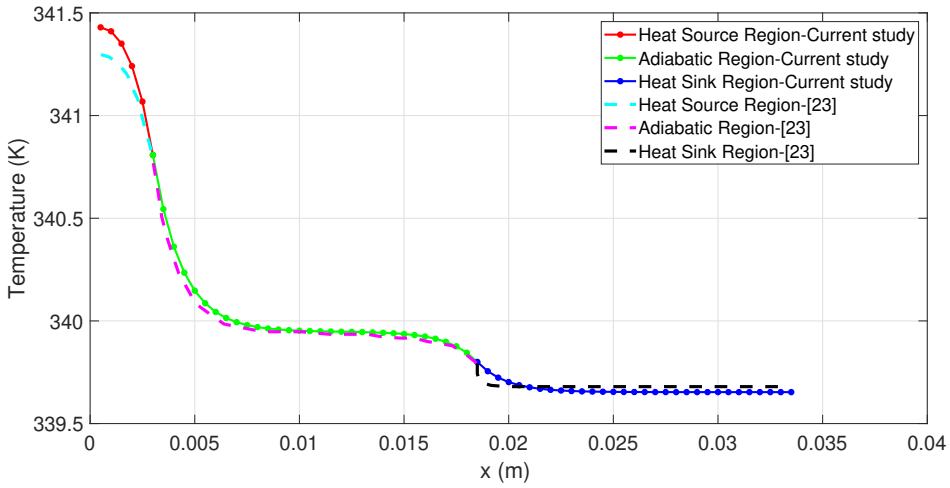

Figure 4.2: Temperature distribution comparison, $\hat{\sigma} = 0.03$

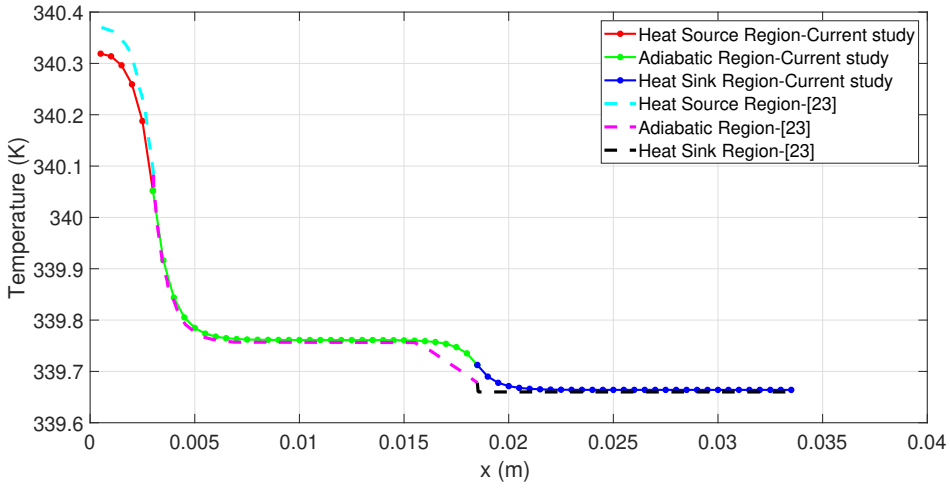

Figure 4.3: Temperature distribution comparison, $\hat{\sigma} = 1$

As shown in Figure 4.2 and Figure 4.3, temperature distribution on outer walls of the vapor chamber is compared. The results show that outer wall temperature distribution

values of the current study and benchmark study have in good agreement. In addition to that, Table 4.2 shows the comparison for temperature difference and liquid pressure drop in the wick according to different accommodation coefficient values.

Table 4.2: Comparison the benchmark study [23] and current study

Model	**$\hat{\sigma}$ = 0.03**		**$\hat{\sigma}$ = 1**	
	Temperature difference (°C)	**Liquid pressure drop (Pa)**	**Temperature difference (°C)**	**Liquid pressure drop (Pa)**
Benchmark study [23]	1.62	320	0.73	323
Current study	1.77	327	0.65	335
Difference (%)	9.2	2.1	10.9	3.7

These results show that because of the smaller value of the accommodation coefficient, the thermal resistance of the liquid–vapor interface within the vapor chamber is substantial, which ultimately results in the vapor chamber having a greater thermal resistance. Therefore, increasing accommodation coefficient results a decrease in the value of temperature drop on the exterior walls of the vapor chamber.

4.2 Parametric Study

The performance of the vapor chamber is affected by a number of significant aspects, including the dimensions, outside conditions, heat source parameters, and materials used in the vapor chamber. In this section, a parametric study is performed to see the effects of parameters on the vapor chamber characteristics.

The maximum operating temperatures for conventional electronic components are typically set at around 80°C–85°C for industrial applications. As an example, the I7 CPU from Intel is required to function at temperatures no higher than 85 °C [47]. Therefore, in this parametric study, the maximum allowable temperature is set at 85°C.

For the parametric study, properties as shown in Table 4.3 are used in simulated models. Effective wick thermal conductivity and permeability values are calculated as mentioned in Sections 2.4 and 2.5, respectively. Also note that, porosity value is taken 0.5 for all parametric studies except the section of porosity effect. Surface tension is temperature dependent property which is shown in Figure 3.8, and this is calculated according to temperature distribution of the vapor chamber and then, capillary pressure value is calculated.

Table 4.3: Parametric study vapor chamber properties

Parameter	**Value**
Length (mm)	30
Height (mm)	3
Heat source size (mm)	5
Wall thickness (mm)	0.25
Wick thickness (mm)	0.2
Wick type	Sintered sphere wick
Pore radius (mm)	0.005
Accommodation coefficient	0.03
Coolant temperature (K)	298
Ambient heat transfer coefficient ($\mathrm{W}/(\mathrm{m}^2 \cdot \mathrm{K})$)	400

4.2.1 Dry-out Condition Investigation of the Benchmark Study

To investigate the dry-out condition, which is mentioned in Section 2.6 for benchmark study, the heat flux value is increased until the liquid pressure drop exceeds the capillary pressure. After this point, the vapor chamber cannot work properly because there is not enough driving force for the liquid within the wick structure. As shown in Figure 4.4a, when heat flux becomes 42.4 W/cm^2, the overall liquid pressure drop begins to be greater than the capillary pressure head. This means that dry-out occurs at this point. On the other side, Figure 4.4b shows that when heat flux becomes larger than 15 W/cm^2, maximum wall temperature exceeds the maximum allowable temper-

ature. As a result, with given these operating conditions, the benchmark study only is able to work properly at 15 W/cm^2 or less than this value .

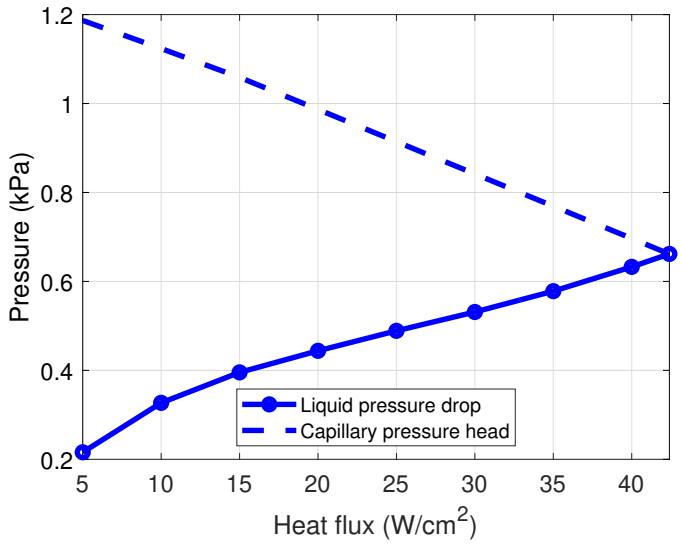

(a) Heat flux effect on pressure drop for the benchmark study

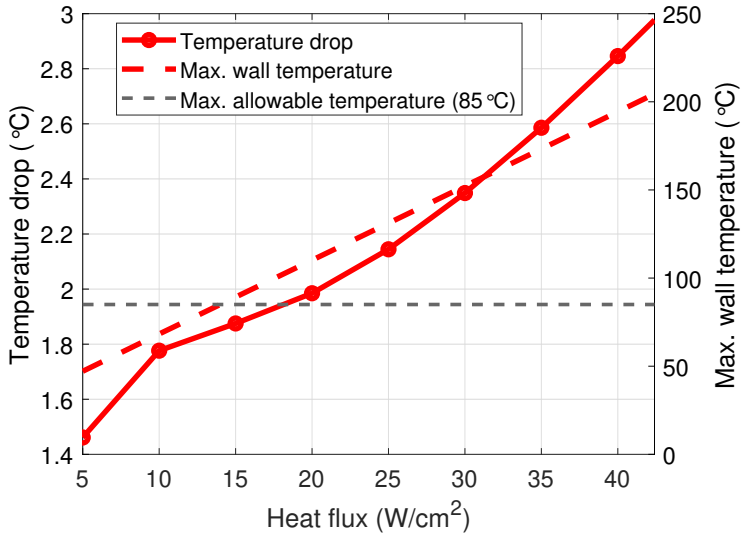

(b) Heat flux effect on temperature drop for the benchmark study

Figure 4.4: Heat flux effect in the benchmark study

4.2.2 Permeability Range Used in Vapor Chambers

In this study, sintered sphere wick as a wick type is used. The permeability calculation as shown in Equation 4.1 is used for sintered sphere wick types. Capillary pressure is calculated as shown in Equation 4.2 where r_p is pore radius. Figure 4.5 shows the plot of permeability as a function of porosity and pore radius. In literature, wick permeability range for vapor chamber models or applications is taken between $10^{-12} < K < 10^{-10}$. To satisfy this permeability condition, porosity and pore radius values can be taken as (0.45, 0.6) and (30μm, 52μm), respectively. In the remainder of the parametric investigation, pore radius is taken as 50 μm, and the porosity value is chosen to match the permeability range. In accordance with that porosity value is chosen as 0.5 except the porosity effect section in which three different porosity values are used.

$$K = \frac{r_p^2 \varepsilon^3}{37.5(1-\varepsilon)^2} \tag{4.1}$$

$$\Delta P_c = \frac{2\sigma}{r_p} \cos\theta \tag{4.2}$$

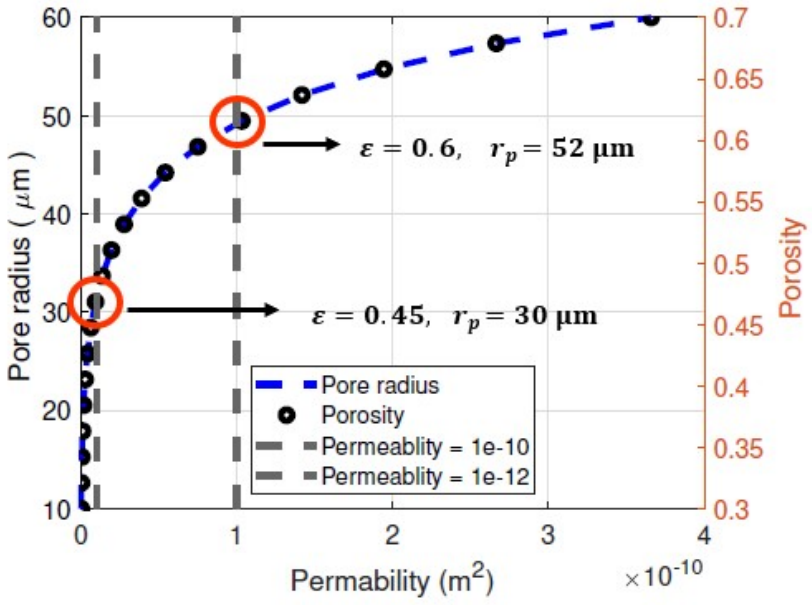

Figure 4.5: Permeability as a function of effective pore radius and porosity

4.2.3 Effect of Porosity

To investigate the effect of different porosity values on pressure and temperature drop and maximum wall temperature, three different porosity values, 0.45, 0.5, and 0.55 are used according to determined range in Figure 4.5. In each porosity value, heat flux given to the system is increased until the dry-out condition is reached as shown in Figure 4.6a. The permeability and the effective thermal conductivity of the wick are both influenced in this way by the porosity values. As a direct consequence of this fact, the thermal and fluid performance characteristics of the vapor chamber will be affected. Figure 4.6a shows that the system's dry-out heat flux values will increase slightly when the porosity value increases. According to Equation 3.22 and Equation 4.1, the permeability is also going up as a result of this, the amount of liquid pressure drop decreases in the system.

When the porosity increases, the effective thermal conductivity of the wick decreases, according to Equation 2.2. However, there is not a significant change in the effective thermal conductivity, so Figure 4.6b shows that there is not much of a change in the maximum wall temperature and temperature drop in the system when the porosity increases.

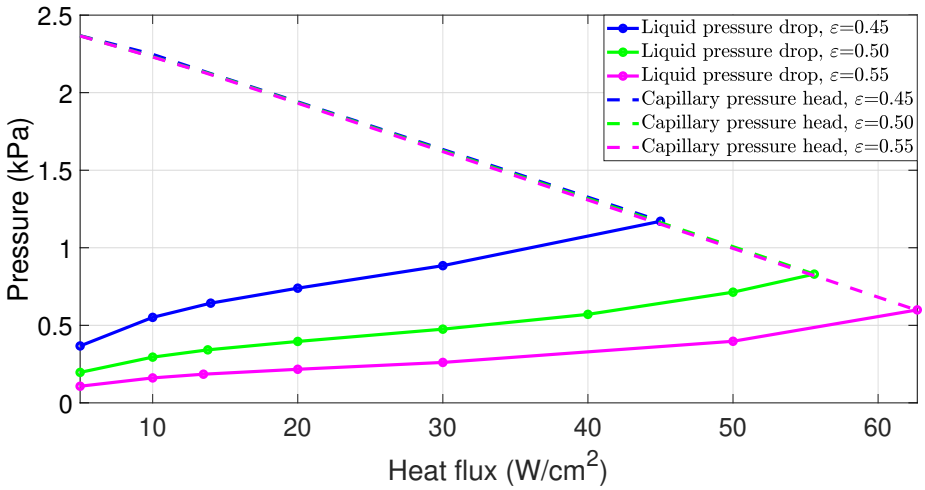

(a) Heat flux effect on pressure drop for different porosity values

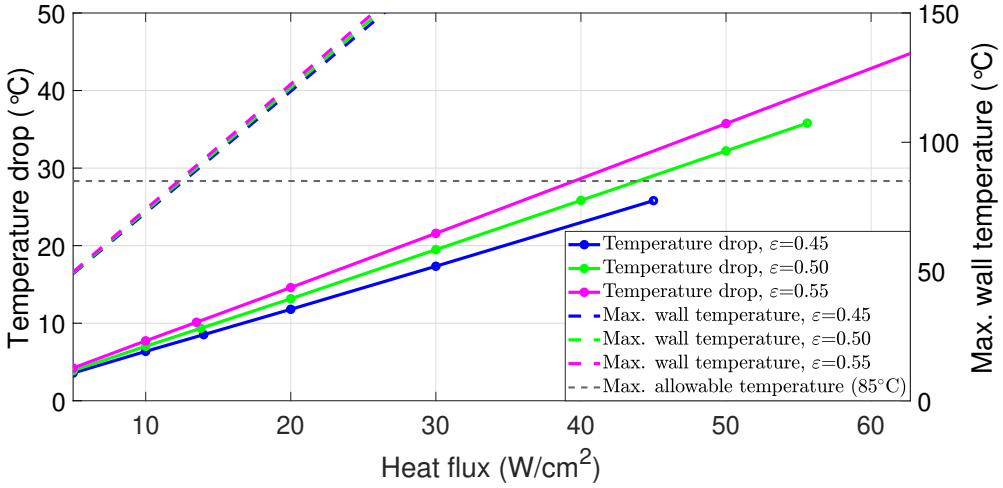

(b) Heat flux effect on pressure drop for different porosity values

Figure 4.6: Heat flux effect for different porosity values

4.2.4 Effect of Wick Thickness

The wick is a crucial part of the vapor chamber because the working fluid is transported by capillary pressure, so properties of the wick affect the liquid flow resistance. The thickness of the wick is also related to how well it moves heat because of how it affects thermal resistance. As shown in Figure 4.7a, the wick is closely related to the friction to liquid flow due to its porous structure. As the thickness of the wick increases, the resistance to liquid flow drop will decrease, and this will result in reducing the pressure drop within the wick structure.

As indicated in Figure 4.7b, an increase in the wick thickness results in an increase in the maximum temperature of the system. This is due to an increase in both temperature of the vapor and the interface heat transfer coefficient between the wick and the vapor as well as the increased thermal resistance of the wick region. On the other hand, it can be seen that there is neither a dry-out heat flux nor a critical heat flux value that causes the maximum temperature to be exceeded. Therefore, the wick thickness value that provides minimum temperature drop might be chosen as a design parameter.

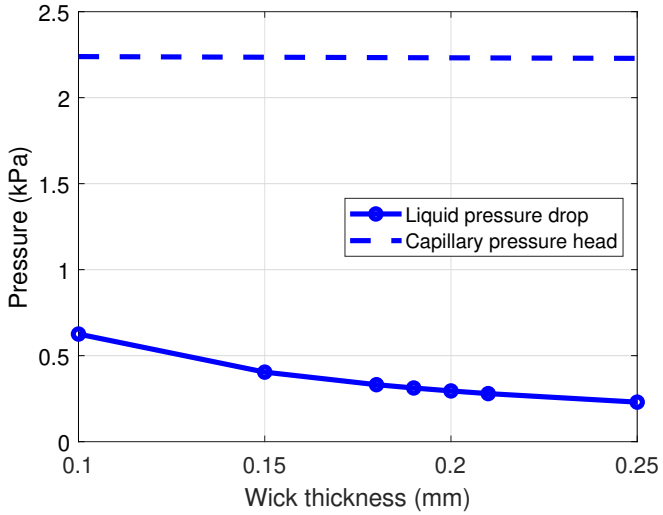

(a) Wick thickness effect on pressure

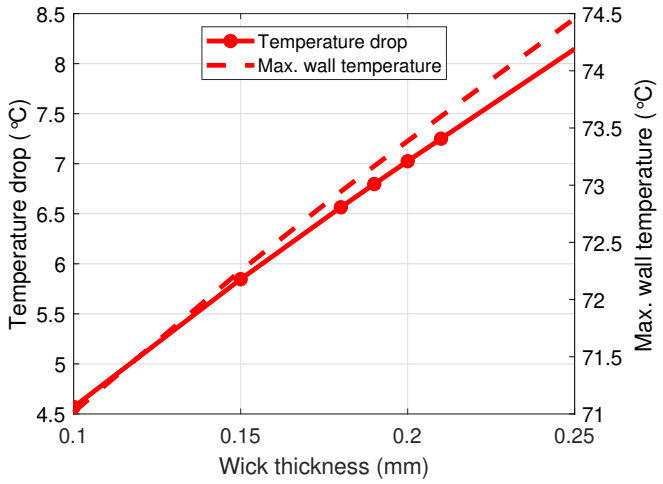

(b) Wick thickness effect on temperature

Figure 4.7: Wick thickness effect in the system, q'' =10 W/cm^2

4.2.5 Effect of Wall Thickness

The wall thickness of the vapor chamber is related to how efficiently heat is transported in both the axial and lateral directions. Figure 4.8a shows that the liquid pressure drop of the vapor chamber is not much affected by changes in wall thickness because there is no capillary or driving force for the working fluid by the wall. Minor variation in the liquid pressure drop is observed due to small changes in temperature and temperature related variables such as density and viscosity. Figure 4.8b shows that the maximum temperature of the vapor chamber is decreased as the thickness of the wall increases. This is because both the vapor temperature and the interface heat transfer coefficient between the wick and the vapor region decrease. As a design parameter, the wall thickness value can be set as high as possible to keep the temperature drop in the system to a minimum.

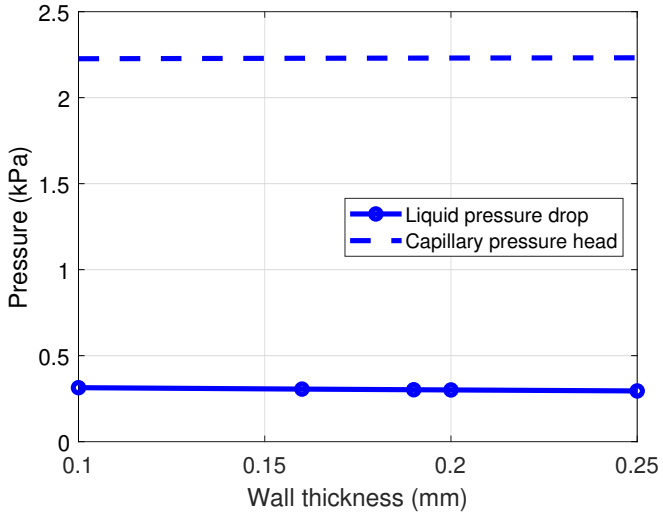

(a) Wall thickness effect on pressure drop

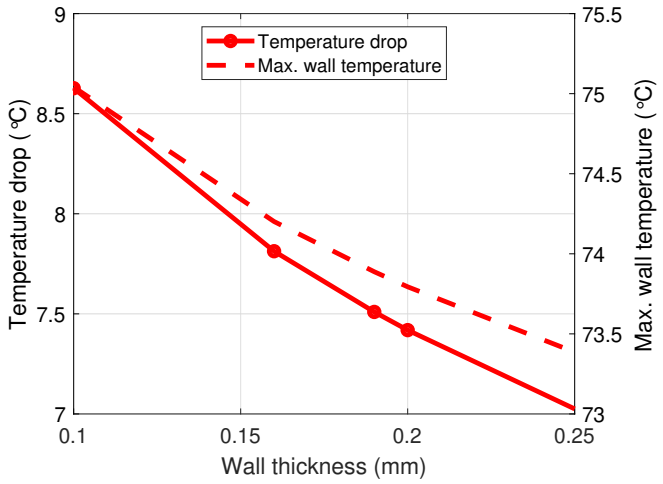

(b) Wall thickness effect on temperature

Figure 4.8: Wall thickness effect in the system, q'' =10 W/cm^2

4.2.6 Effect of Wall Material

Copper is employed as a wall material, nothwithstanding earlier parametric tests. In this section, the effect of different wall material types is investigated. In addition to copper material; silicon, nickel and stainless steel are used as wall material by considering with compatibility water. Thermal conductivities of copper, silicon, nickel and stainless steel are 387.6 $\mathrm{W}/(\mathrm{m}\cdot\mathrm{K})$, 230 $\mathrm{W}/(\mathrm{m}\cdot\mathrm{K})$, 91 $\mathrm{W}/(\mathrm{m}\cdot\mathrm{K})$ and 15 $\mathrm{W}/(\mathrm{m}\cdot\mathrm{K})$, respectively. When the liquid pressure drop for copper is compared to the liquid pressure drop of the other materials as indicated in Figure 4.9a, copper has relatively largest dry-out heat flux value due to its high thermal conductivity value. Therefore, if the copper is used as a wall material, the system can capable of carrying out more heat flux until its allowable temperature value. This conclusion can be seen in Figure 4.9b. As a result, copper can be chosen as a wall material in the vapor chamber design because it has highest dry-out heat flux value. Furthermore, if the same heat flux is applied to the system for each wall type, copper has the lowest maximum wall temperature as well as the lowest temperature and liquid pressure drop of the system.

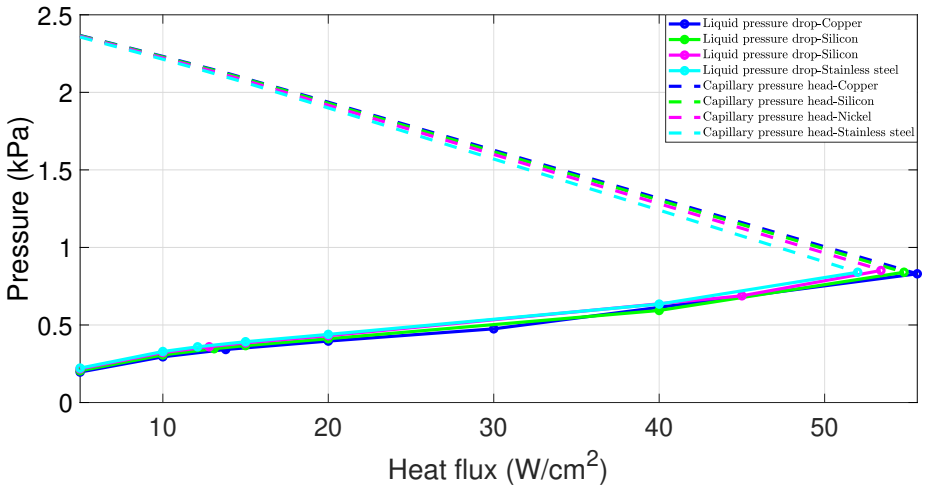

(a) Heat flux effect on pressure drop for wall material types

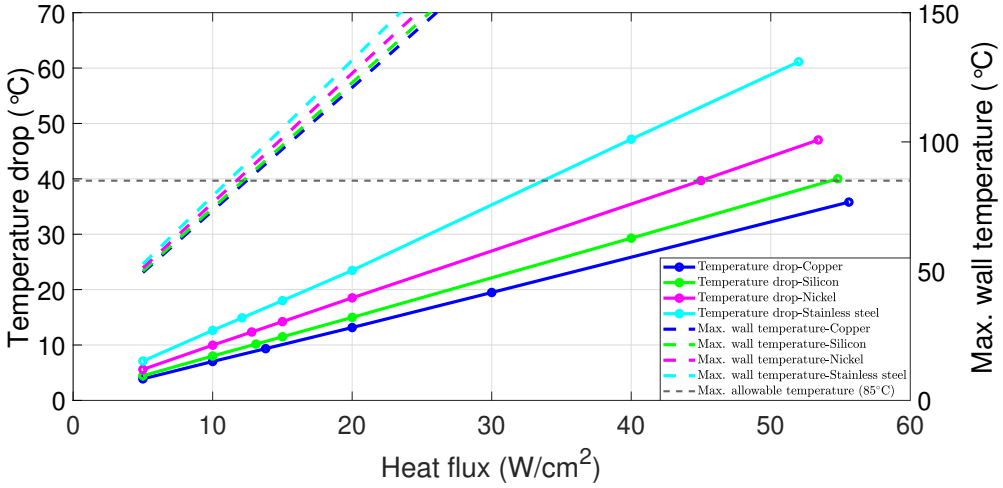

(b) Heat flux effect on temperature drop for wall material types

Figure 4.9: Heat flux effect on wall material types

4.2.7 Effect of Different Working Fluid and Material Types

In Section 2.3, Table 2.2 shows the working fluid and its compatible material types. In the current study, in addition to the investigation of copper-water in previous studies as well as the benchmark study, methanol-copper, aceton-copper, and ammonia-aluminum are chosen for a parametric study to see what happens to the pressure drop and temperature change of the liquid in the system. These types of working fluid and material couples are commonly used in heat pipes and vapor chambers [29,30,48,49]. Another advantage of using aluminum as a wall material over copper is its lighter weight, due to the fact that ammonia-aluminum is the most commonly used for spacecraft thermal management [50]. Because of this feature, the vapor chamber can operate a lighter-weight application.

Among the working fluid and material couples, as shown in Figure 4.10a, acetone-copper has the highest dry-out heat flux value which is around 12 W/cm^2 but this amount of heat flux exceeds the maximum allowable temperature as indicated in Figure 4.10b, so under this heat flux, the vapor chamber cannot perform properly. On the other side, Figure 4.10b shows that acetone-copper has the largest temperature drop in the system. Ammonia-aluminum couple has the minimum temperature drop at dry-out heat flux compared to the others as shown in Figure 4.10b. Figure 4.10a shows that methanol-copper has the lowest dry-out heat flux which is around 7.9 W/cm^2. These three working fluid and wick material couples can be compared with copper-water which is used in previous parametric sets. Figure 4.10a shows that dry-out heat flux value is around 55 W/cm^2 but this causes exceeding the maximum allowable temperature. Maximum heat flux that can be given to the system without exceeding the operating temperature and causing dry-out condition is around 13 W/cm^2. Also, copper-water has the smallest temperature drop in the system for each heat flux value compared to other working fluid-wick material couples. As a conclusion, among four of them, copper-water is the best option for a vapor chamber design in terms of the smallest temperature drop and maximum dry-out heat flux value to operate reliably.

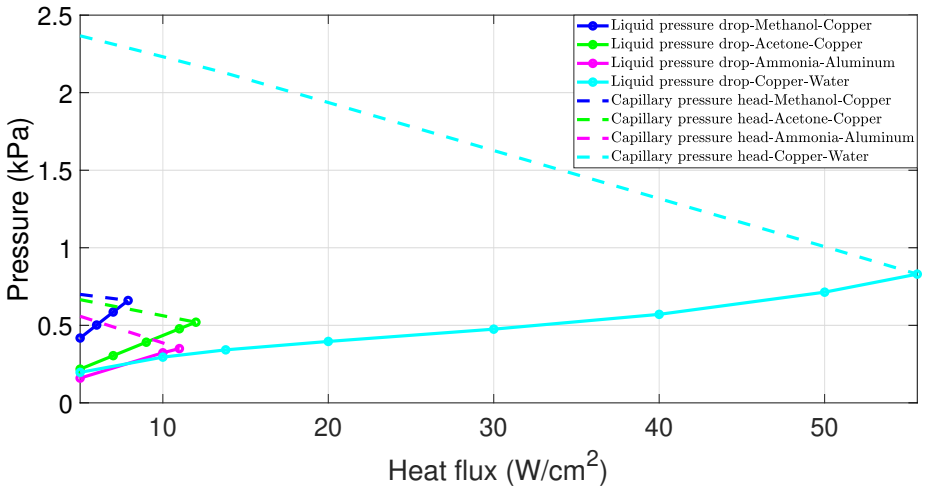

(a) Heat flux effect on pressure drop for different working fluids and material types

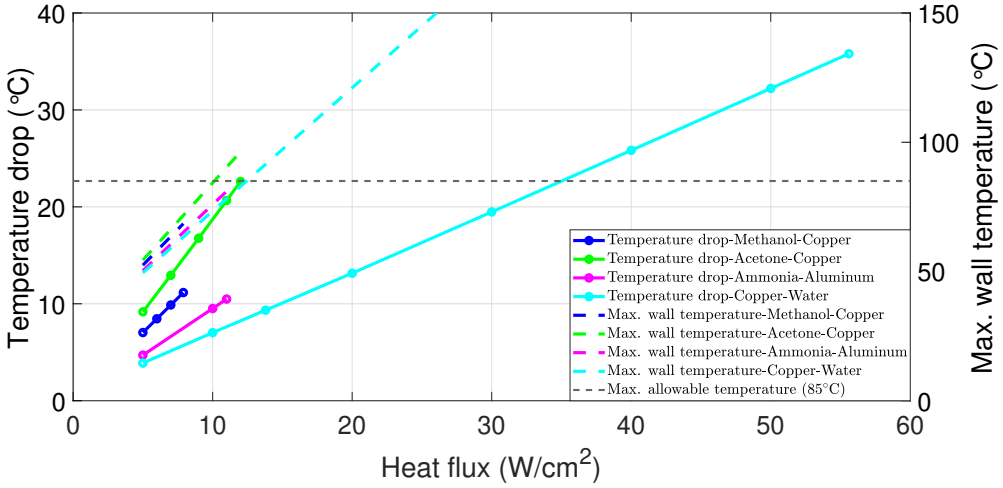

(b) Heat flux effect on temperature drop for different working fluids and material types

Figure 4.10: Heat flux effect on different working fluid and material type

CHAPTER 5

CONCLUSION AND SUGGESTIONS FOR FUTURE WORK

This thesis presents the numerical modeling and investigation of a vapor chamber design. The modeling approach that is now being used is helpful in designing a vapor chamber by taking into account all of the relevant properties to explore the parameters. For this, one-dimensional modeling is utilized. Through this model, parametric studies are performed. The model is validated with the benchmark study [23] which includes the CFD study of the vapor chamber. The effects of all parameters on the liquid pressure drop, the maximum wall temperature, and the temperature drop of the vapor chamber are studied.

According to parametric study results, increasing the porosity value of the wick structure causes an increase in the temperature drop of the system as well as a decrease in the liquid pressure drop due to the increased permeability of the wick. Also, when the porosity increases, the system's dry-out heat flux value will increase slightly. Increasing wick thickness results in an increase in the maximum temperature of the system due to the increased vapor temperature and interface heat transfer coefficient. Also, as the thickness of the wick increases, the pressure drop caused by the velocity of the liquid goes down.

In terms of the wall thickness effect, changes in wall thickness have little effect on the vapor chamber's liquid pressure drop. As the thickness of the wall increases, the maximum temperature of the vapor chamber decreases. This is due to a drop in both the vapor temperature and the interface heat transfer coefficient between the wick and the vapor region.

In the benchmark study, copper is used as a wall material. Also, in the parametric

study section, different material types such as silicon, nickel, and stainless steel are used by considering with compatibility water. Because copper has a relatively high dry-out heat flux value, it can be used as a wall material in the vapor chamber design. Furthermore, when the same heat flux is given to the system for each wall type, copper has the lowest maximum wall temperature as well as the system's lowest temperature and liquid pressure drop.

Depending on the requirements of the application, a specific type of working fluid and/or material may be required. Besides water-copper working fluid and material type couple, effects of different working fluids and material types are investigated. Accordingly, methanol-copper, aceton-copper, and ammonia-aluminum are chosen to evaluate their influence on the system's liquid pressure drop and temperature change. In terms of the smallest temperature drop and maximum dry-out heat flux value, copper-water is a better option for a vapor chamber design. However, when compared to aluminum, copper has a disadvantage in terms of weight. As a result, aluminum is the superior material, particularly for spacecraft thermal management. In this particular type of application, the use of ammonia-aluminum would be preferable.

As a future study, the next step would be to design an experimental setup so that real-world data can be compared to the computational data that was found in this study. In addition to that, in the present investigation, there is a single heat source located in the center of the vapor chamber, and its heat flux is constant. This boundary condition can be periodic in a future development. Additionally, the number of heat sources can be adjusted, and the effects of both single and multiple sources can be examined. Because the heat provided fluctuates with time during the operation of electronic equipment, it is essential to analyze the periodic situation. Finally, the modeling that is being done right now is based on the cartesian coordinate system, but this can be changed to a radial coordinate system because radial geometry is more suitable for the applications that are being used.

REFERENCES

[1] J. Wei, "Challenges in cooling design of cpu packages for high-performance servers," *Heat Transfer Engineering*, vol. 29, no. 2, p. 178–187, 2008.

[2] R. M. Viswanath and V. S. Wakharkar, "Thermal performance challenges from silicon to systems 1 thermal performance challenges from silicon to systems," 2000.

[3] P. Naphon, S. Wiriyasart, and S. Wongwises, "Thermal cooling enhancement techniques for electronic components," *International Communications in Heat and Mass Transfer*, vol. 61, p. 140–145, 2015.

[4] B. Liu, "Vapor chamber external and internal factors investigation," Master's thesis, University of California, Irvine, 2020.

[5] C. Byon, "Heat pipe and phase change heat transfer technologies for electronics cooling," *Electronics Cooling*, 2016.

[6] G. M. Grover, "Evaporation-condensation heat transfer device," Patent US3 229 759A.

[7] K. N. Shukla, "Heat pipe for aerospace applications—an overview," *Journal of Electronics Cooling and Thermal Control*, vol. 05, no. 01, p. 1–14, 2015.

[8] S. Han, L. Yang, Z. Tian, X. Yuan, and H. Lu, "Research on a simplified model of an aluminum vapor chamber in a heat dissipation system," *Entropy*, vol. 22, no. 1, p. 35, 2019.

[9] T. Nguyen, M. Mochizuki, K. Mashiko, Y. Saito, and I. Sauciuc, "Use of heat pipe/heat sink for thermal management of high performance cpus," *Sixteenth Annual IEEE Semiconductor Thermal Measurement and Management Symposium (Cat. No.00CH37068)*.

[10] H. B. Ma and G. P. Peterson, "The influence of the thermal conductivity on the heat transfer performance in a heat sink," *Journal of Electronic Packaging*, vol. 124, no. 3, p. 164–169, 2002.

[11] R. S. Prasher, "A simplified conduction based modeling scheme for design sen-

sitivity study of thermal solution utilizing heat pipe and vapor chamber technology," *Journal of Electronic Packaging*, vol. 125, no. 3, p. 378–385, 2003.

[12] U. Vadakkan, S. V. Garimella, and J. Y. Murthy, "Transport in flat heat pipes at high heat fluxes from multiple discrete sources," *Journal of Heat Transfer*, vol. 126, no. 3, p. 347–354, 2004.

[13] X. Wei and K. Sikka, "Modeling of vapor chamber as heat spreading devices," *Thermal and Thermomechanical Proceedings 10th Intersociety Conference on Phenomena in Electronics Systems, 2006. ITHERM 2006.*

[14] Y. Wang and K. Vafai, "Transient characterization of flat plate heat pipes during startup and shutdown operations," *International Journal of Heat and Mass Transfer*, vol. 43, no. 15, p. 2641–2655, 2000.

[15] S.-S. Hsieh, R.-Y. Lee, J.-C. Shyu, and S.-W. Chen, "Analytical solution of thermal resistance of vapor chamber heat sink with and without pillar," *Energy Conversion and Management*, vol. 48, no. 10, p. 2708–2717, 2007.

[16] Y. Koito, H. Imura, M. Mochizuki, Y. Saito, and S. Torii, "Numerical analysis and experimental verification on thermal fluid phenomena in a vapor chamber," *Applied Thermal Engineering*, vol. 26, no. 14-15, p. 1669–1676, 2006.

[17] Z. Ming, L. Zhongliang, and M. Guoyuan, "The experimental and numerical investigation of a grooved vapor chamber," *Applied Thermal Engineering*, vol. 29, no. 2-3, p. 422–430, 2009.

[18] N. Zhu and K. Vafai, "Vapor and liquid flow in an asymmetrical flat plate heat pipe: A three-dimensional analytical and numerical investigation," *International Journal of Heat and Mass Transfer*, vol. 41, no. 1, p. 159–174, 1998.

[19] G. Patankar, J. A. Weibel, and S. V. Garimella, "On the transient thermal response of thin vapor chamber heatnbsp;spreaders: Optimized design and fluid selection," *International Journal of Heat and Mass Transfer*, vol. 148, p. 119106, 2020.

[20] G. Carbajal, C. Sobhan, G. Peterson, D. Queheillalt, and H. Wadley, "Thermal response of a flat heat pipe sandwich structure to a localized heat flux," *International Journal of Heat and Mass Transfer*, vol. 49, no. 21-22, p. 4070–4081, 2006.

[21] J. Rice and A. Faghri, "Analysis of screen wick heat pipes, including capillary

dry-out limitations," *Journal of Thermophysics and Heat Transfer*, vol. 21, no. 3, p. 475–486, 2007.

[22] P. Naphon and S. Wiriyasart, "On the thermal performance of the vapor chamber with micro-channel for unmixed air flow cooling," *Engineering Journal*, vol. 19, no. 1, p. 125–137, 2015.

[23] R. Ranjan, J. Y. Murthy, S. V. Garimella, and U. Vadakkan, "A numerical model for transport in flat heat pipes considering wick microstructure effects," *International Journal of Heat and Mass Transfer*, vol. 54, no. 1-3, p. 153–168, 2011.

[24] R. K. Bumataria, N. Chavda, and H. Panchal, "Current research aspects in mono and hybrid nanofluid based heat pipe technologies," *Heliyon*, vol. 5, no. 5, 2019.

[25] Y. Li, Z. Li, W. Zhou, Z. Zeng, Y. Yan, and B. Li, "Experimental investigation of vapor chambers with different wick structures at various parameters," *Experimental Thermal and Fluid Science*, vol. 77, p. 132–143, 2016.

[26] J. L. Velardo, "Thermal performance investigation of vapour chamber heat spreader," Ph.D. dissertation, RMIT University, September 2019.

[27] M. Lu, L. Mok, and R. J. Bezama, "A graphite foams based vapor chamber for chip heat spreading," *Journal of Electronic Packaging*, vol. 128, no. 4, p. 427–431, 2005.

[28] Y.-T. Chen, S.-W. Kang, Y.-H. Hung, C.-H. Huang, and K.-C. Chien, "Feasibility study of an aluminum vapor chamber with radial grooved and sintered powders wick structures," *Applied Thermal Engineering*, vol. 51, no. 1-2, p. 864–870, 2013.

[29] X. Ji, J. Xu, and A. M. Abanda, "Copper foam based vapor chamber for high heat flux dissipation," *Experimental Thermal and Fluid Science*, vol. 40, p. 93–102, 2012.

[30] S.-C. Wong, S.-F. Huang, and K.-C. Hsieh, "Performance tests on a novel vapor chamber," *Applied Thermal Engineering*, vol. 31, no. 10, p. 1757–1762, 2011.

[31] A. Faghri, "Heat pipes: Review, opportunities and challenges," *Frontiers in Heat Pipes*, vol. 5, no. 1, 2014.

[32] H. Hassan and S. Harmand, "Parametric study of the effect of the vapor chamber characteristics on its performance," *Journal of Heat Transfer*, vol. 135, no. 11, 2013.

[33] A. Faghri, *Heat Pipe Science and Technology*. Taylor and Francis, 1995.

[34] W. Wnek, J. Ramshaw, J. Trapp, E. Hughes, and C. Solbrig, "Transient three-dimensional thermal-hydraulic analysis of nuclear reactor fuel rod arrays: General equations and numerical scheme," 1975.

[35] A. Bejan and A. D. Kraus, *Heat Transfer Handbook*. Wiley, 2003.

[36] M. T. Ababneh, F. M. Gerner, P. Chamarthy, P. d. Bock, S. Chauhan, and T. Deng, "Thermal-fluid modeling for high thermal conductivity heat pipe thermal ground planes," *Journal of Thermophysics and Heat Transfer*, vol. 28, no. 2, p. 270–278, 2014.

[37] D. A. Reay, *Heat pipes: Theory, design and applications*. Butterworth Heinemann, 2006.

[38] R. Giraudon, S. Lips, D. Fabrègue, L. Gremillard, E. Maire, and V. Sartre, "Effect of the wick characteristics on the thermal behaviour of a lhp capillary evaporator," *International Journal of Thermal Sciences*, vol. 133, p. 22–31, 2018.

[39] S. W. Chi, "Heat pipe theory and practice: A sourcebook," 1977.

[40] M. Čarnogurská, M. Příhoda, T. Brestovič, J. Molínek, and R. Pyszko, "Determination of permeability and inertial resistance coefficient of filter inserts used in the cleaning of natural gas," *Journal of Mechanical Science and Technology*, vol. 26, no. 1, p. 103–111, 2012.

[41] R. R. Williams and D. K. Harris, "Cross-plane and in-plane porous properties measurements of thin metal felts: Applications in heat pipes," *Experimental Thermal and Fluid Science*, vol. 27, no. 3, p. 227–235, 2003.

[42] B. Holley and A. Faghri, "Permeability and effective pore radius measurements for heat pipe and fuel cell applications," *Applied Thermal Engineering*, vol. 26, no. 4, p. 448–462, 2006.

[43] C. Oshman, "Development, fabrication, and experimental study of flat polymer micro heat pipes," 2012.

[44] B. Zohuri, "Basic principles of heat pipes and history," *Heat Pipe Design and Technology*, p. 1–41, 2016.

[45] J. Rose, "Interphase matter transfer, the condensation coefficient and dropwise condensation, in:," *Proceedings of the 11th International Heat Transfer Conference, Kyongju, Korea*, vol. 1, p. 89–104, 1998.

[46] V. Badam, V. Kumar, F. Durst, and K. Danov, "Experimental and theoretical investigations on interfacial temperature jumps during evaporation," *Experimental Thermal and Fluid Science*, vol. 32, no. 1, p. 276–292, 2007.

[47] D. Chou, "Infrastructure," *Practical Guide to Clinical Computing Systems*, p. 39–70, 2015.

[48] S. Peyghambarzadeh, S. Shahpouri, N. Aslanzadeh, and M. Rahimnejad, "Thermal performance of different working fluids in a dual diameter circular heat pipe," *Ain Shams Engineering Journal*, vol. 4, no. 4, p. 855–861, 2013.

[49] K. Yang, Y. Mao, Z. Cong, and X. Zhang, "Experimental research of novel aluminium-ammonia heat pipes," *Procedia Engineering*, vol. 205, p. 3923–3930, 2017.

[50] Z. Li, "Design and preliminary experiments of a novel heat pipe using a spiral coil as capillary wick," *International Journal of Heat and Mass Transfer*, vol. 126, p. 1240–1251, 2018.